Reversible Reorganization Of Basolateral Amygdala Dendrites in Male Rats Accompanies Stress Resilience

Sheldon D. Michaelson[1], Ana Pamela Miranda Tapia[1], Amanda McKinty[1], Heika Silveira Villarroel[1], James P. Mackay[1], Janice H. Urban[2], William F. Colmers[1,3*]

[1] Department of Pharmacology, and the Neuroscience and Mental Health Institute, University of Alberta, Edmonton, Alberta, T6G 2H7, Canada

[2] Center for the Neurobiology of Stress Resilience and Psychiatic Disorders; Discipline of Physiology and Biophysics, Chicago Medical School, Rosalind Franklin University of Medicine and Science, North Chicago, IL, 60064 USA

[3]Lead contact.

***Corresponding Author:** Dr. William F. Colmers, Department of Pharmacology and Institute for Neuroscience and Mental Health, University of Alberta, 9-36 MSB, Edmonton, AB. T6G 2H7, Canada. wcolmers@ualberta.ca

Number of Figures: 13

Number of Tables : 2

Number of words in Abstract: 147

ABSTRACT

Basolateral amygdala (BLA) responses to stress are regulated by endogenous neuropeptide Y (NPY) and corticotrophin-releasing factor (CRF), associated respectively with resilience and vulnerability to stress. We studied mechanisms underlying effects of repeated NPY and CRF treatment on structure and function of BLA principal neurons (PN) in organotypic slice cultures (OTC) of rat BLA. NPY attenuated excitatory input and induced dendritic hypotrophy via Y_5-receptors, while CRF increased excitatory input and induced hypertrophy of BLA PNs. Structural responses to NPY and CRF required calcineurin and CaMKII, respectively. Finally, repeated *in vivo* treatment of BLA with NPY or a Y_5 receptor agonist increased social interaction and recapitulated structural changes in BLA neurons seen in OTCs. These results implicate the Y_5 receptor in the long-term, anxiolytic-like effects of NPY in the BLA. Moreover, BLA OTCs offer a robust model to study mechanisms associated with resilience and vulnerability to stress in BLA.

Keywords: Organotypic slice cultures; Basolateral amygdala; Stress resilience; Neuropeptide Y; CRF, dendritic plasticity, Social interaction

40 **INTRODUCTION**

41 Acute stress elicits a coordinated, adaptive response to real or perceived threats, which is
42 soon terminated via neural and endocrine systems that buffer the stress and restore homeostasis.
43 While the stress response is essential to survival, persistent or extreme stress can disrupt this
44 balance, predisposing the individual to maladaptive, affective- and anxiety-related disorders
45 (McEwan, 2003). Stress-related signals are processed in part through the complex network of
46 inhibitory and excitatory neurons in the amygdala, particularly the basolateral amygdala (BLA),
47 which receives input related to stress, emotion and memory (Phelps and Ledoux, 2005). BLA
48 projections, in turn, control and modulate anxiety-, reward- and emotionally-driven behaviors
49 (McDonald, 1985, McDonald et al., 1989). Extreme or prolonged stress can overwhelm this
50 homeostatic control, resulting in an imbalance between the glutamatergic excitatory and
51 GABAergic inhibitory control of BLA activity, and enhancing not only the anxiogenic output of
52 BLA projection neurons (Roozendaal et al., 2009), but causing hypertrophy of their dendritic
53 arbors, accompanied by increased numbers of excitatory synaptic spines (Mitra et al., 2005, Padival
54 et al., 2013, Adamec et al., 2012, Hill et al., 2011, Vyas et al., 2002, 2006). Such changes can persist
55 for weeks (Vyas et al., 2004).

56 In addition to GABA and glutamate, the neuropeptides corticotropin-releasing factor (CRF)
57 and Neuropeptide Y (NPY) provide regulation of the BLA, with CRF being excitatory and NPY
58 inhibitory to BLA activity. While CRF is associated with the generation of stress responses (Rainnie
59 et al., 2004; Sajdyk et al., 2004) NPY is an important endogenous anxiolytic compound in rodents
60 (Sajdyk et al., 2002, 2004) and in humans where NPY is also linked to resilience (Yehuda et al.,
61 2006; Sajdyk et al., 2008; Zhou et al., 2008). These behavioral effects of NPY are linked to some
62 of its actions within the amygdala, as administration of NPY decreases the activity of BLA PNs

63 through activation of NPY Y_1 receptors (Y_1R), which acutely hyperpolarizes and inhibits BLA PNs
64 through suppression of somatodendritic I_h (Giesbrecht et al., 2010). Moreover, NPY acutely
65 decreases BLA activity by enhancing $GABA_A$-mediated inhibitory postsynaptic currents (IPSCs),
66 and reducing NMDA-mediated excitatory postsynaptic currents (EPSCs) (Molosh et al., 2013) in
67 BLA PNs.

68 Together a balance between CRF and NPY signaling within the BLA is important for
69 various behavioral responses (Sajdyk et al., 2004; Heilig 1994; 2004; Gutman et al., 2008). When
70 subjected to a stressor, CRF is released to generate an appropriate behavioral stress response (e.g.,
71 freezing, fleeing), these neural and behavioral responses are in turn buffered by NPY release which
72 temporally occurs after the stressor to curtail the actions of CRF and limit the duration of the stress
73 response (Heilig et al., 1994). A predominance of either NPY or CRF tone can tip this balance and
74 induce anxiolysis and anxiogenesis, respectively (Sajdyk et al., 2004, Heilig et al., 1994). This
75 balance is maintained in part through differential modulation of the tonically-active H-current (I_h):
76 CRF acutely depolarizes and excites BLA PNs by enhancing the (I_h), whereas NPY suppresses I_h
77 in the same neurons (Giesbrecht et al, 2010). Subjecting animals to either repeated stress (Padival
78 et al, 2013) or daily injections of urocortin (UCN- a CRF-R1 and CRF-R2 agonist) induces anxiety
79 that long outlasts the stimulus; conversely, generation of a persistent stress resilience is generated
80 by a similar treatment with NPY (Sajdyk et al,, 2008, Rainnie et al., 2004). In all, these cellular
81 responses likely underlie the ability of NPY to mitigate CRF- and stress-induced, BLA-mediated
82 behaviors (Sajdyk et al., 2006; Rainnie et al., 2004).

83 As repeated injections of CRF produce stress vulnerability (increased sensitivity to stressful
84 situations; Rainnie et al., 2004), repeated application of NPY induces a persistent stress resilience
85 that lasts for at least two months (Sajdyk et al., 2008). Resilience is defined as the ability to rebound

86 from trauma or severe stress and is associated with positive mental health outcomes (Yehuda et al.,
87 2006). Using these models provides a unique opportunity to identify and exploit molecular and
88 cellular mechanisms associated with neuroplasticity in the BLA associated with stress-related
89 behavioral outcomes. We recently showed that a reduction in I_h in BLA PNs contributes to, and
90 mimics, this long-term resilience (Silveira Villarroel et al., 2018). Beyond this however, the cellular
91 mechanisms mediating long-term NPY and CRF effects on BLA neurons, which drive adaptive and
92 maladaptive coping strategies to stress exposure are poorly understood, in part because acute brain
93 slice preparations, while useful, are short-lived. To get around this issue, organotypic slice cultures
94 (OTCs) derived from hippocampus, spinal cord and cerebellum have been shown to reliably retain
95 gross tissue organization, properties of synaptic transmission, neuronal morphology and
96 neurochemical phenotypes (De Simoni et al., 2003, Avossa et al., 2003, Lu et al., 2009, Gähwiler,
97 1981) permitting comparison and validation relative to acute slice preparations (De Simoni et al.,
98 2003, Gähwiler, 1981, Stoppini et al., 1991). Moreover, OTCs permit the rigorous study of chronic
99 treatments and long-term effects of acute manipulations in a well-defined system (Humpel, 2015).
100 Here we report OTC preparations containing the BLA, a novel *in vitro* model in which to study
101 stress-related circuitry and more clearly understand the interactions of NPY and CRF and the
102 mechanisms underlying their persistent regulation of BLA PN output.

103 We found that repeated incubations of BLA-OTCs with NPY, designed to mimic *in vivo*
104 NPY injection protocols that induce stress resilience (Sajdyk et al., 2008, Silveira Villarroel et al.,
105 2018), reduced synaptic excitation and increased inhibition of PNs and induced a persistent, marked
106 hypotrophy of their dendritic trees. Structural effects of NPY were mediated entirely by NPY_5
107 receptors (Y_5R), and were calcineurin-dependent. Similar incubations with CRF resulted in effects
108 opposite to those of NPY that were mediated by CaMKII; treatment with either peptide reversed or

109 prevented the effects of the other. Finally, repeated *in vivo* injections of NPY or of Y_5R-selective
110 agonists into the BLA not only induced an enduring state of behavioral stress resilience, but also
111 replicated the dendritic remodeling seen in BLA OTCs, an action mediated entirely by the Y_5R.
112 These studies indicate a novel structural correlate of persistent stress resilience, and highlight the
113 use of the BLA OTC model in identifying mechanisms of adaptive and maladaptive coping
114 strategies to stress and anxiety-like behavior.

115 **RESULTS**

116 **Repeated NPY and CRF treatments cause dendritic hypotrophy and hypertrophy,**
117 **respectively, in OTC PNs**

118 Repeated restraint stress induces lasting dendritic hypertrophy in BLA neurons (Padival et
119 al., 2013). Whereas *in vivo* administration of CRF into the BLA elicits long-term stress
120 vulnerability, NPY administration persistently decreases the animals' vulnerability to stress (Sajdyk
121 et al., 2008, Rainnie et al., 2004, Silveira Villarroel et al., 2018). The persistence of NPY's effects
122 may parallel the persistence of the stress-induced dendritic hypertrophy in BLA neurons (Padival
123 et al., 2013), but mechanisms underlying the effects of either endogenous neuropeptide remain
124 unclear. To test our hypothesis that repeated application of either NPY or CRF to BLA OTCs will
125 alter electrophysiological properties of PNs and result in their respective hypotrophy or
126 hypertrophy, we monitored PN properties with electrophysiology and post-recording
127 morphological analysis. Initial validation of the OTC preparation of BLA (Material and Methods)
128 included an extensive comparision of PN neuronal properties with neurons from acute *ex vivo* brain
129 slices of P14 and P70 animals **(Table 1)**; the PNs from OTCs were more compact but electrically
130 more similar to those from acute slices from the adult animals.

131 Repeated application of NPY (1 – 100 nM) reduced PN whole-cell capacitance relative to
132 vehicle controls (**Fig. 1a**). Consistent with this, NPY (≥ 1 nM) reduced and simplified the dendritic
133 arbor (**Fig. 1b-j**), decreasing the total dendritic length (**Fig. 1b**) and complexity of dendritic
134 branching (**Fig. 1c,d**). NPY's effects on dendritic morphology were already significant at 1 nM (p
135 <0.0001 vs. control). Although dendritic spine density was not altered by 100 nM NPY, estimates
136 of total spine numbers showed a trend toward reduction compared to controls (**Fig. 2**), consistent
137 with the significant reduction in EPSC frequencies observed (**Fig. 3b,c,e**). Neurons treated with the
138 inactive, desamido NPY analogue (daNPY – 100 nM) (Wahlestedt et al., 1986), did not differ in
139 any aspect from untreated controls (**Fig. 1a-f**).

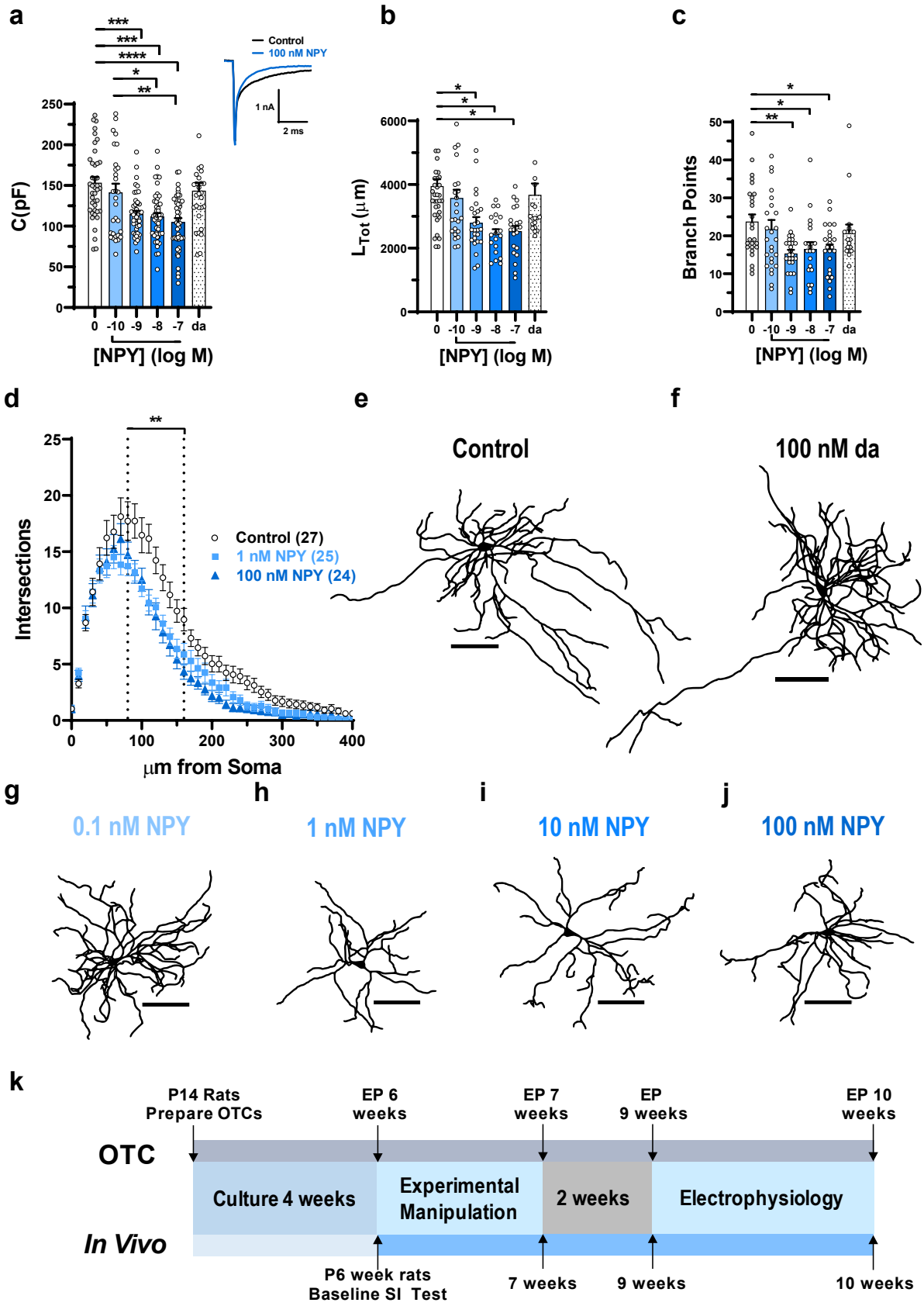
a
b
c
C(pF)
Control
100 nM NPY
1 nA
2 ms
L_{Tot} (μm)
Branch Points
[NPY] (log M)
0 -10 -9 -8 -7 da
d
e
f
Intersections
μm from Soma
Control (27)
1 nM NPY (25)
100 nM NPY (24)
Control
100 nM da
g
h
i
j
0.1 nM NPY
1 nM NPY
10 nM NPY
100 nM NPY
k
P14 Rats
Prepare OTCs
EP 6
weeks
EP 7
weeks
EP
9 weeks
EP 10
weeks
OTC
Culture 4 weeks
Experimental
Manipulation
2 weeks
Electrophysiology
In Vivo
P6 week rats
Baseline SI Test
7 weeks
9 weeks
10 weeks

140

141 **Figure 1. NPY treatment of BLA OTC causes pyramidal neuron hypotrophy.** **a**. Scatter plot of
142 mean capacitance of OTC pyramidal neurons treated with vehicle ("Control" n=42), NPY at 100
143 pM (n=31), 1 nM (n=43), 10 nM (n=47), 100 nM (n=49) and the inactive analogue, desamido-NPY
144 at 100 nM ("da" n=30) ($H_{(5)}$ = 40.72, p =1.07e^{-7}). ***Inset*** Representative capacitative transients for
145 control- or 100 nM NPY-treated BLA OTC neurons. **b**. Scatter plot of mean total dendritic length
146 for OTC neurons treated as in **a**. Vehicle (n=26), NPY at 100 pM (n=26), 1 nM (n=25), 10 nM (n=21),
147 100 nM (n=24) and da-NPY 100 nM (n=20) ($H_{(5)}$ = 19.04, p = 0.0019). **c.** Scatter plot of mean number
148 of branch points in neurons in **b** ($H_{(5)}$ = 17.02, p = 0.0045). **d**. Sholl analysis of neurons in **b** and **c**
149 treated as indicated (Treatment: $F_{(2, 72)}$ = 9.96, p = 0.00015; Distance: $F_{(40, 2880)}$ = 185.4, p ~ 0;
150 Interaction: $F_{(80, 2880)}$ = 2.09, p =8.57e^{-8}). **e-j.** Representative reconstructions of neurons treated as
151 indicated above. **k.** Comparative timelines for experiments with BLA OTCs (upper timeline) and *in*
152 *vivo* (lower timeline) models. N-values for **c** and **d** are as in **b**. For **a-c**, Kruskal-Wallis H tests with
153 Dunn's post hoc tests. For **d**, 2-way RM ANOVA with Tukey's post-hoc test. For **a-c**, circles
154 represent neurons, black bars represent population means, while in **d**, symbols represent
155 population means and for all, error bars indicate s.e.m. All tests were two-sided. **P*<0.05,
156 ***P*<0.01, ****P*<0.001, *****P*<0.0001 for post hoc multiple comparisons. Scale bars in e-j = 100
157 µm.

158

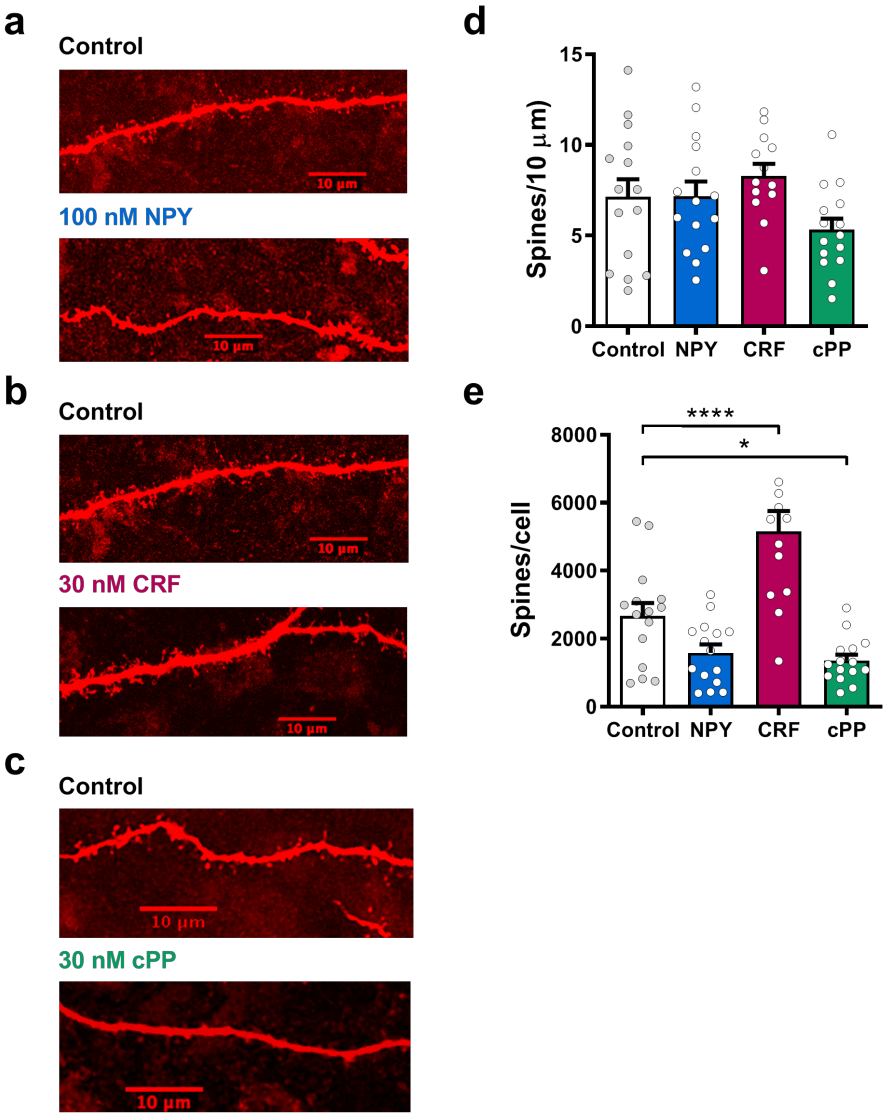

Figure 2. Treatment with NPY, CRF or the Y_5R agonist, cPP, affects the estimated total number of spines per cell, but not spine density of principal neurons in BLA OTCs. a – c.. Representative images of spines on pyramidal neurons treated with vehicle control, 100 nM NPY, 100 nM cPP and 30 nM CRF, as indicated. **d**. Scatter plot of mean spine density of pyramidal neurons treated as in **a**. vehicle control (n=15), 100 nM NPY (n=15), 100 nM cPP (n=15) and 30 nM CRF (n=15); 1-way ANOVA with Dunnett's multiple comparisons test: $F_{(3, 56)} = 1.437$, $p = 0.24$. **e**. Scatter plot of mean estimated total number of spines for neurons in **d** (One-way ANOVA with Welch's correction and Dunnett's T3 multiple comparisons test $W_{(3, 29.15)} = 10.61$, $p = 7.09e^{-5}$). For **d,e,** circles represent neuron means, black bars represent population means and for all, error bars indicate s.e.m. All tests were two-sided. *P<0.05, **P<0.01, ***P<0.001, ****P<0.0001.

171

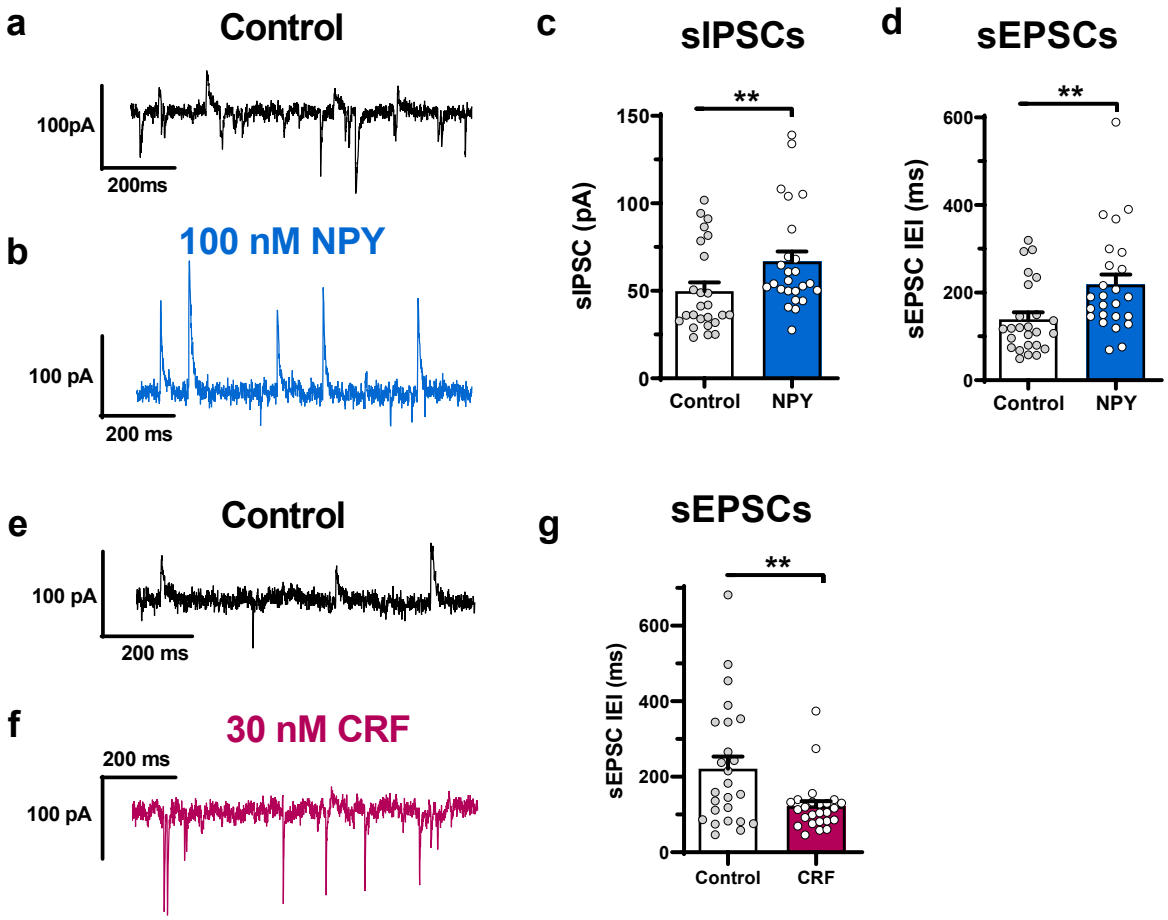

172

173 **Figure 3. Changes in principal neuron synaptic properties with repeated NPY or CRF treatment**
174 **in BLA OTCs. a – b** Representative electrophysiological recordings of spontaneous synaptic
175 currents in BLA OTC principal neurons treated repeatedly with vehicle (**a)** and (**b**) 100 nM NPY, **c**.
176 Mean sIPSC amplitudes in neurons in vehicle control (n=25) or 100 nM NPY (n=25) (Mann-Whitney
177 U test; U = 171.0, *p* = 0.0054). **d**. Scatter plots of mean sEPSC interevent interval from recordings
178 of cells in **c.** Vehicle control (n=25) or 100 nM NPY (n=25) (Mann-Whitney U test; U = 155.5, *p* =
179 0.0019) **e – f** Representative electrophysiological recordings of neurons treated repeatedly with
180 vehicle or with 30 nM CRF **g**. Mean sEPSC interevent interval in vehicle control (n=25) or 100 nM
181 30 nM CRF (n=25). (Mann-Whitney U test; U = 194, *p* = 0.0208). For **c,d, g**, circles represent neuron
182 means, black bars represent population means and for all, error bars indicate s.e.m. All statistical
183 tests were two-sided. **P<0.01.

184 Repeated treatment of OTCs with CRF induced a diametrically opposite set of changes in
185 BLA PN physiology and structure. Thus, application of 30 nM CRF increased sEPSC frequency
186 compared to vehicle-treated PNs (**Fig. 3 f-h**). Furthermore, compared with controls, CRF increased

whole-cell capacitance (**Fig. 4a**) and caused hypertrophy of the dendritic arbor (**Fig. 4b**), including increased branching (**Fig. 4c**) and dendritic complexity (**Fig. 4d-g**). The effects of CRF on dendritic morphology occurred in a more clearly concentration-dependent manner than did those of NPY. Although CRF-treatment did not alter spine density, estimates of total spine numbers were significantly increased compared to controls (**Fig. 2**).

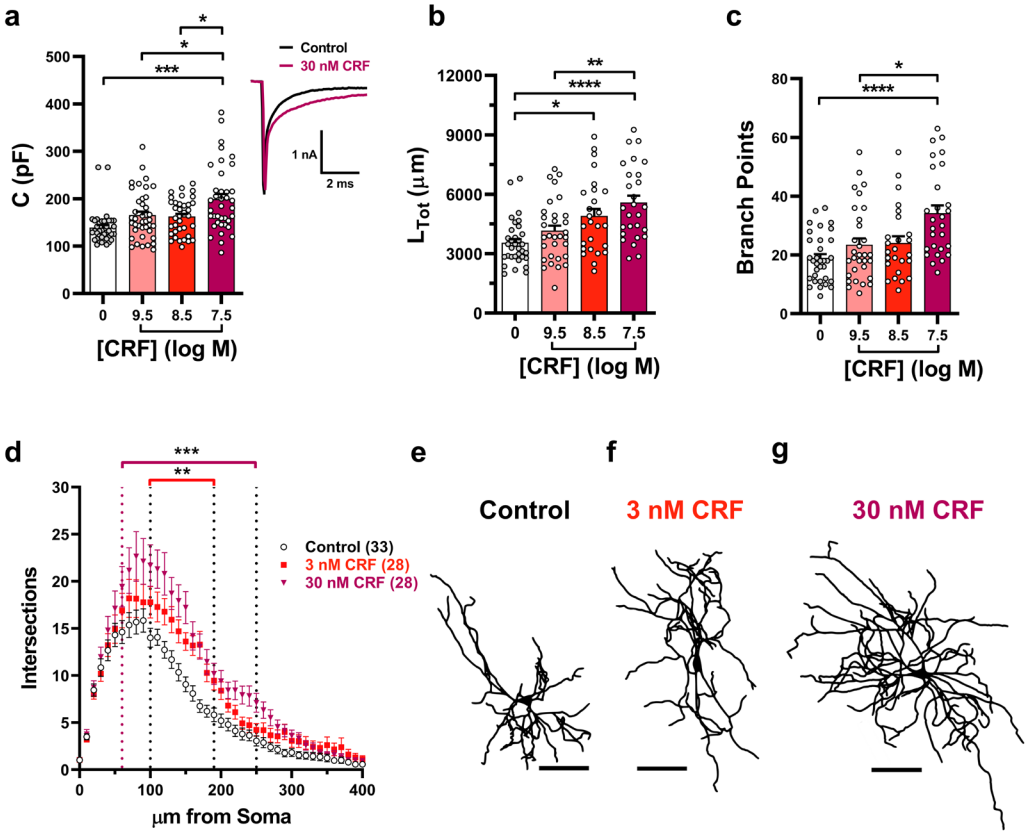

Figure 4. CRF treatment of BLA OTC causes pyramidal neuron hypertrophy. a. Scatter plot of mean capacitance of OTC pyramidal neurons treated with vehicle control (n=39) and CRF at 300 pM (n=40), 3 nM (n=36) and 30 nM (n=38) ($H_{(3)}$ = 22.67, p = 4.72e^{-5}). ***Inset***. Representative capacitance transients from control- or 30 nM CRF-treated BLA OTC neurons. **b.** Scatter plot of mean total dendritic length for OTC neurons treated as in **a**. Vehicle control (n=33) and CRF at 300 pM (n=31), 3 nM (n=26) and 30 nM (n=28) ($H_{(3)}$ = 22.71, p =4.63e^{-5}). **c**. Scatter plot of mean number of branch points in neurons in **b** ($H_{(3)}$ = 19.90, p = 0.0002). **d**. Sholl analysis of neurons in **b** and **c** treated as indicated (<u>Treatment:</u> $F_{(2, 84)}$ = 11.43, p = 4.05e^{-5}; <u>Distance:</u> $F_{(40, 3360)}$ = 137.4, p ~ 0; <u>Interaction:</u> $F_{(80, 3360)}$ = 2.58, p = 1.45e^{-12}). **e**-**g**. Representative reconstructions of neurons treated

202 as indicated above. For **a-c**, Kruskal-Wallis H tests with Dunn's post hoc tests. For **d**, 2-way RM
203 ANOVA with Tukey's post-hoc test. For **a-c**, circles represent neurons, black bars represent
204 population means, while in **d**, symbols represent population means and for all, error bars indicate
205 s.e.m. All tests were two-sided. *P<0.05, **P<0.01, ***P<0.001, ****P<0.0001 for post hoc
206 multiple comparisons. Scale bars in e-g = 100 µm

207

208 **Bi-directional PN dendritic remodeling after successive treatments with NPY and CRF in**
209 **BLA OTCs**

210 BLA output, and thus the physiological and behavioral responses to stress are governed in
211 part by the opposing actions of NPY and CRF neuropeptide systems. Disruption of this homeostatic
212 mechanism may in part underlie some persistent anxiety-related disorders (Schmeltzer et al., 2016).
213 We therefore next determined if NPY and CRF can also act as counter-regulatory signals in BLA
214 OTCs.

215 BLA OTCs were incubated for one week with either CRF or NPY, then some were
216 incubated the following week respectively with either NPY or CRF, and maintained in control
217 media for one additional week (**Fig. 5a**) before electrophysiological and morphological analyses
218 were performed on both single- and double-treated populations. Specifically, when PNs were
219 reciprocally treated with the two peptides in either order, there were no differences either in cell
220 capacitance (**Fig. 5a**) or dendritic size or complexity (**Fig. 5b-g**) from vehicle controls. As in the
221 previous experiments, application of NPY or CRF alone either decreased or increased the frequency
222 of sEPSCs observed in the OTCs, whereas sEPSC frequency in the CRF,NPY- or NPY,CRF-treated
223 groups was not significantly different from vehicle controls (**Fig. 5h-k**). Assessment of BLA PN
224 morphology in the CRF,NPY and NPY,CRF groups was consistent with the neurons undergoing a
225 bi-directional structural plasticity.

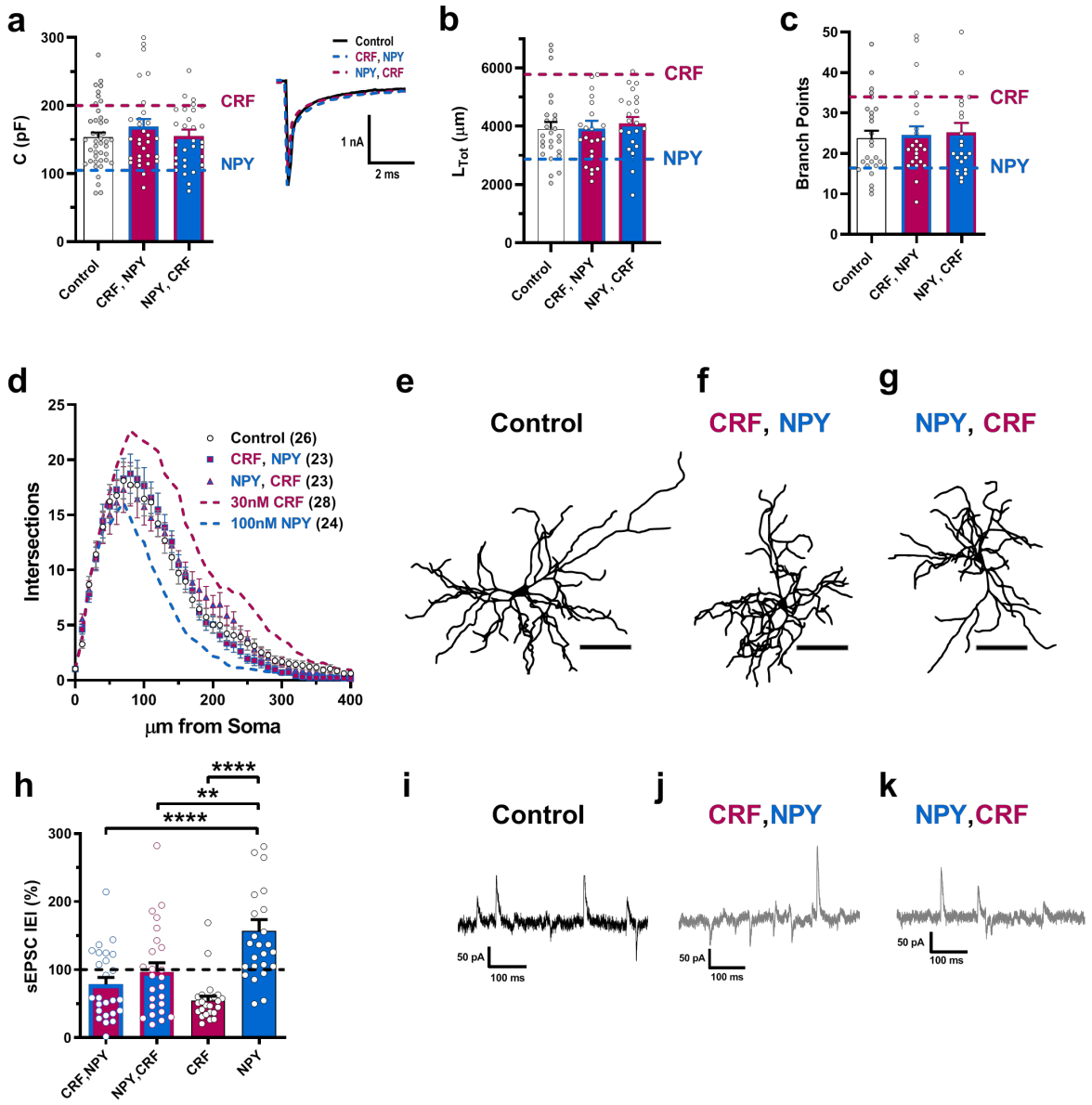

226

227 **Figure 5. Sequential treatment with NPY or CRF reverses or prevents the effects of each**
228 **neuropeptide alone on BLA OTC pyramidal neuron morphology. a**. Scatter plot of mean
229 capacitance of OTC pyramidal neurons treated with media control (n=42), 30 nM CRF followed by
230 100 nM NPY (n=31) and 100 nM NPY followed by 30 nM CRF (n=32), with the mean capacitance
231 for 30 nM CRF and 100 nM NPY alone (data from figs 1 and 2) indicated by dashed lines ($H_{(2)}$ =
232 0.73, p = 0.69). ***Inset*** Representative capacitance transients from control, CRF, NPY- and NPY, CRF-
233 treated BLA OTC neurons. **b**. Scatter plot of mean total dendritic length for OTC neurons treated
234 as in **a**. with control (n=26), CRF and NPY (n=23) and NPY and CRF (n=23) with the mean total
235 length for 30 nM CRF and 100 nM NPY alone from Figs 1 and 2 as dashed lines ($H_{(2)}$ = 0.80, p =

236 0.67). **c**. Scatter plot of mean number of branch points in neurons in **b** with the mean values for
237 30 nM CRF and 100 nM NPY alone from Figs 1 and 2 as dashed lines ($H_{(2)} = 0.36$, $p = 0.84$). **d**. Sholl
238 analysis of neurons in **b** and **c** with the Sholl analysis for 30 nM CRF and 100 nM NPY from Figs 1
239 and 2 as dashed lines (Treatment: $F_{(2, 69)} = 0.21$, $p = 0.81$; Distance: $F_{(40, 2760)} = 157.3$, $p \sim 0$;
240 Interaction: $F_{(80, 2760)} = 0.70$, $p = 0.98$). **e**-**g**. Representative traces from neurons treated as
241 indicated.. **h.** Mean sEPSC interevent interval in neurons treated with 30 nM CRF followed by 100
242 nM NPY (n=25), 100 nM NPY followed by 30 nM CRF (n=25), 30 nM CRF alone (n=25) and 100 nM
243 NPY alone (n=25) ($H_{(3)} = 28.18$, $p = 3.33e^{-6}$). **i-k** representative recordings from neurons treated as
244 indicated. Statistical tests: For **a-c**, Kruskal-Wallis H tests with Dunn's post hoc tests. For **d**, 2-way
245 RM ANOVA with Tukey's post-hoc tests. For **h**, Kruskal-Wallis H test with Dunn's post hoc test. For
246 **a-c**, circles represent individual neurons, black bars represent population means, while in **d**,
247 symbols represent population means and for all, error bars indicate s.e.m. All statistical tests were
248 two-sided. *P<0.05, **P<0.01, ***P<0.001, ****P<0.0001. Scale bars in e-j = 100 µm.

249

250 **The Y_5R but not the Y_1R mediates dendritic hypotrophy in BLA OTCs**

251 While NPY plays a key role in behavioral stress resilience, the receptor subtype(s) mediating
252 the long-term effect on behavior is unknown. The BLA expresses Y_1, Y_2 and Y_5 NPY receptors
253 (Kopp et al., 2002; Wolak et al., 2003; Stanic et al., 2011) and while the acute anxiolytic effects of
254 NPY in the BLA are mediated predominantly via the Y_1R (Sajdyk et al., 2002a), evidence also
255 suggests a role for the Y_5R (Sajdyk et al., 2002a). Unexpectedly, selective activation of Y_2
256 receptors in the BLA acutely increases PN excitability (Mackay et al., 2019) and facilitates the
257 anomalous expression of anxiety-like behaviors (Sajdyk et al., 2002b). We thus examined the roles
258 of different NPY receptors in a pharmacological experiment using BLA OTCs.

259 In a repeated incubation experiment as with NPY above, the Y_1R-selective agonist, F^7,P^{34}-
260 NPY (1–100 nM) had no measurable long-lasting effects on the properties of BLA OTC PNs
261 compared to controls at any concentration tested. Thus, whole-cell capacitance (**Fig. 6a**), sEPSC
262 frequency (**Fig. 7 a-c**), or any of the morphological parameters affected by NPY itself in this system
263 were unchanged (**Fig. 6b-d**). The Y_2R-selective agonist, $[ahx^{5-24}]NPY^{36}$ (1 – 100 nM; Beck-
264 Sickinger et al, 1992), had only minor effects on the same parameters at lower concentrations, but

265 at higher concentrations (100 nM) we observed a significant increase, relative to vehicle, both in
266 whole-cell capacitance and in dendritic arborization (total dendritic length and number of branches;
267 **Fig. 8a-g**) which was similar to that seen with CRF. These results are consistent with previously
268 reported anxiogenic actions of Y_2 receptor agonists (Sajdyk et al, 2002a,b), and indicate the Y_2
269 receptor is unlikely to mediate NPY-induced hypotrophy.

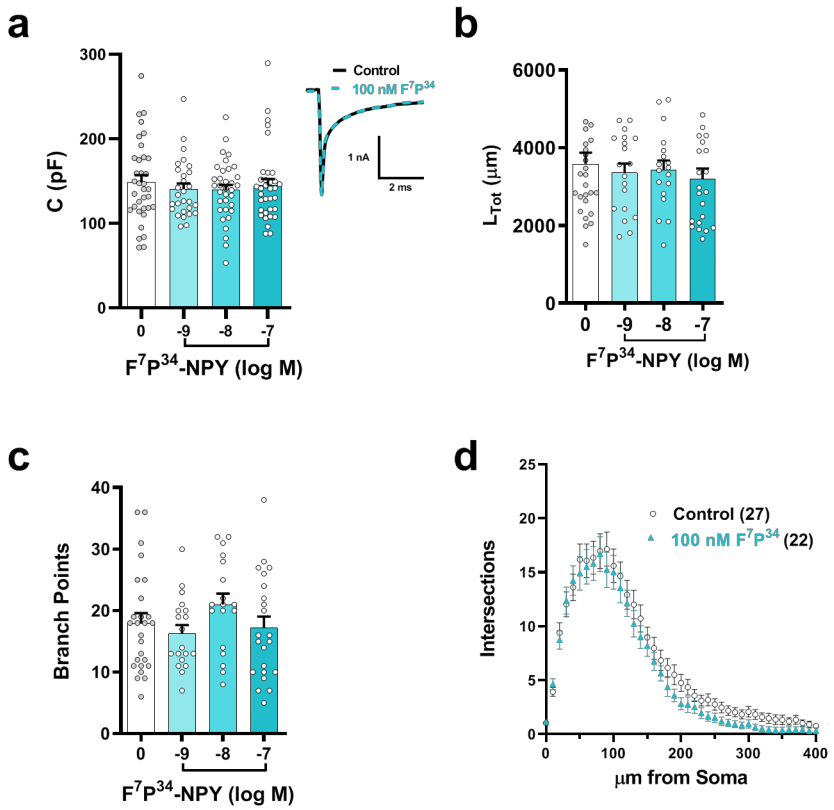

270

271 **Figure 6. Treatment with the selective Y_1 receptor agonist F^7P^{34}-NPY does not affect BLA OTC**
272 **pyramidal neuron morphology. a**. Scatter plot of mean capacitance of OTC pyramidal neurons
273 treated with vehicle control (n=30) and F^7P^{34}-NPY at 1 nM (n=28), 10 nM (n=34) and 100 nM (n=34)
274 ($H_{(3)}$ = 0.58, p = 0.90). ***Inset*** Representative capacitance transients from Control- and F^7P^{34} NPY-
275 treated BLA OTC neurons. **b**. Scatter plot of mean total dendritic length for neurons treated as in
276 **a**. vehicle control (n=27) and F^7P^{34}-NPY at 1 nM (n=19), 10 nM (n=18) and 100 nM (n=22) ($H_{(3)}$ =
277 1.04, p = 0.79). **c**. Scatter plot of mean number of branch points for neurons in **b** ($H_{(3)}$ = 4.25, p =
278 0.24). **d**. Sholl analysis for neurons in **b** and **c** treated as indicated (<u>Treatment:</u> $F_{(1, 48)}$ = 1.82, p =
279 0.18; <u>Distance:</u> $F_{(40, 1920)}$ = 109.3, p ~ 0; <u>Interaction:</u> $F_{(40, 1920)}$ = 0.33, p =0.99). For **a-c**, Kruskal-Wallis

H tests with Dunn's post hoc tests. For **d**, 2-way RM ANOVA with Tukey's post-hoc test. For **a-c**, circles represent neurons, black bars represent population means, while in **d**, symbols represent population means and for all, error bars indicate s.e.m. All tests were two-sided.

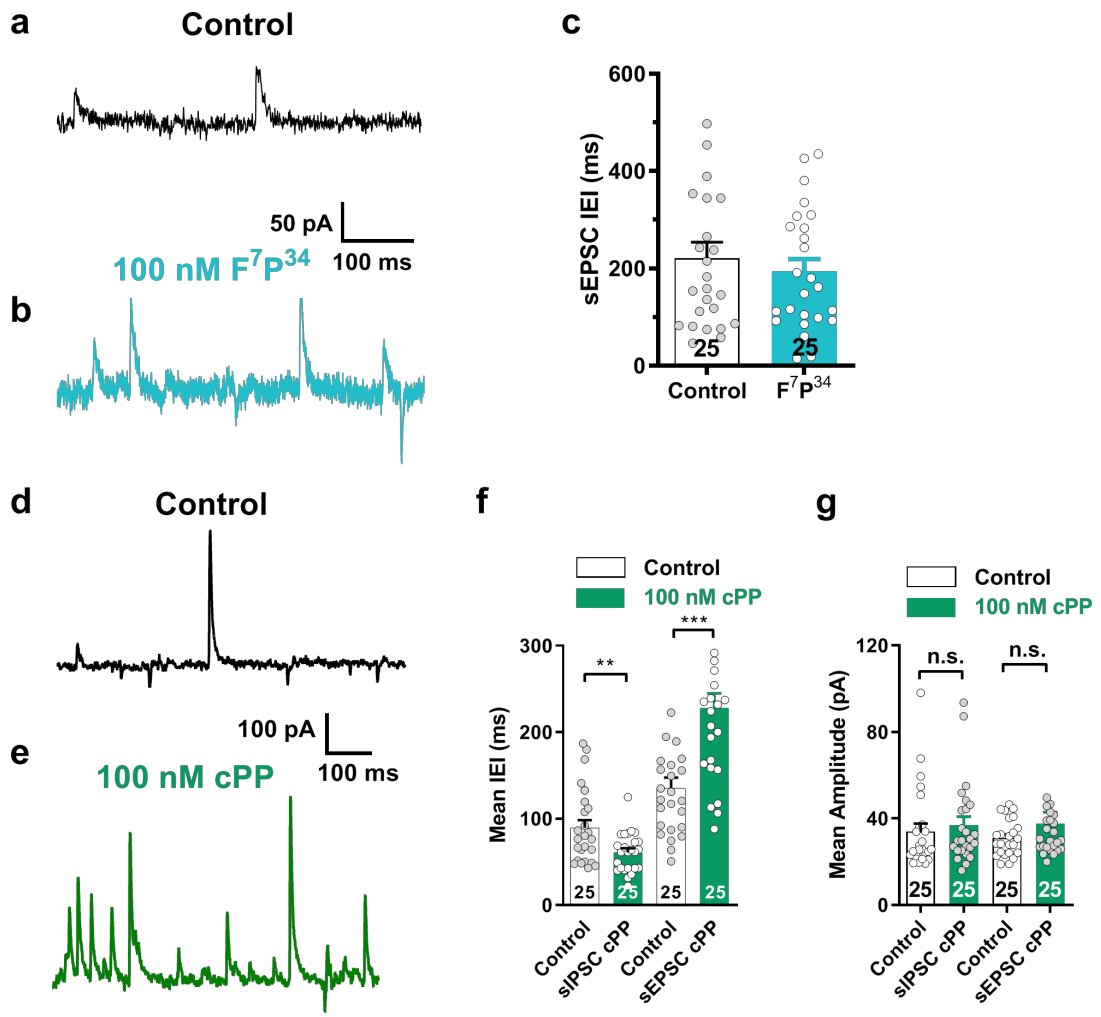

Figure 7. Treatment with the Y_1R agonist F^7P^{34}-NPY does not affect the sEPSC frequency, while the Y_5 agonist cPP reduces sEPSC frequency onto BLA OTC pyramidal neurons. **a-b,d-e**. Representative electrophysiological recordings of spontaneous synaptic currents in BLA OTC pyramidal neurons treated with (**a,d**) vehicle, (**b**) F^7P^{34}- NPYand (**e**) cPP. **c.** Scatter plot of mean interevent sEPSC intervals onto pyramidal neurons treated with vehicle (n=25) and 100 nM F^7P^{34}-NPY (n=25) (Mann-Whitney U test; U = 299.0, p = 0.80). **f.** Scatter plot of mean inter-event interval of sIPSC (t-test with Welch's correction: $t_{(36.20)}$ = 2.92, p = 0.0060) and sEPSCs (Mann-Whitney U test; U = 111.0, p <0.0001) from vehicle control (n=25) and cPP-treated neurons (n=25). **g.** Scatter

plot of mean amplitudes of sIPSC (Mann-Whitney U test; U = 259.0, p =0.30) and sEPSCs (Mann-Whitney U test; U = 269.0, p =0.40) from vehicle control (n=25) and cPP (100 nM)-treated (n=25) neurons. For **c,f-g**, circles represent neuron means, black bars represent population means and for all, error bars indicate s.e.m. All statistical tests were two-sided. ns = P>0.05,*P<0.05, **P<0.01, ***P<0.001, ****P<0.0001.

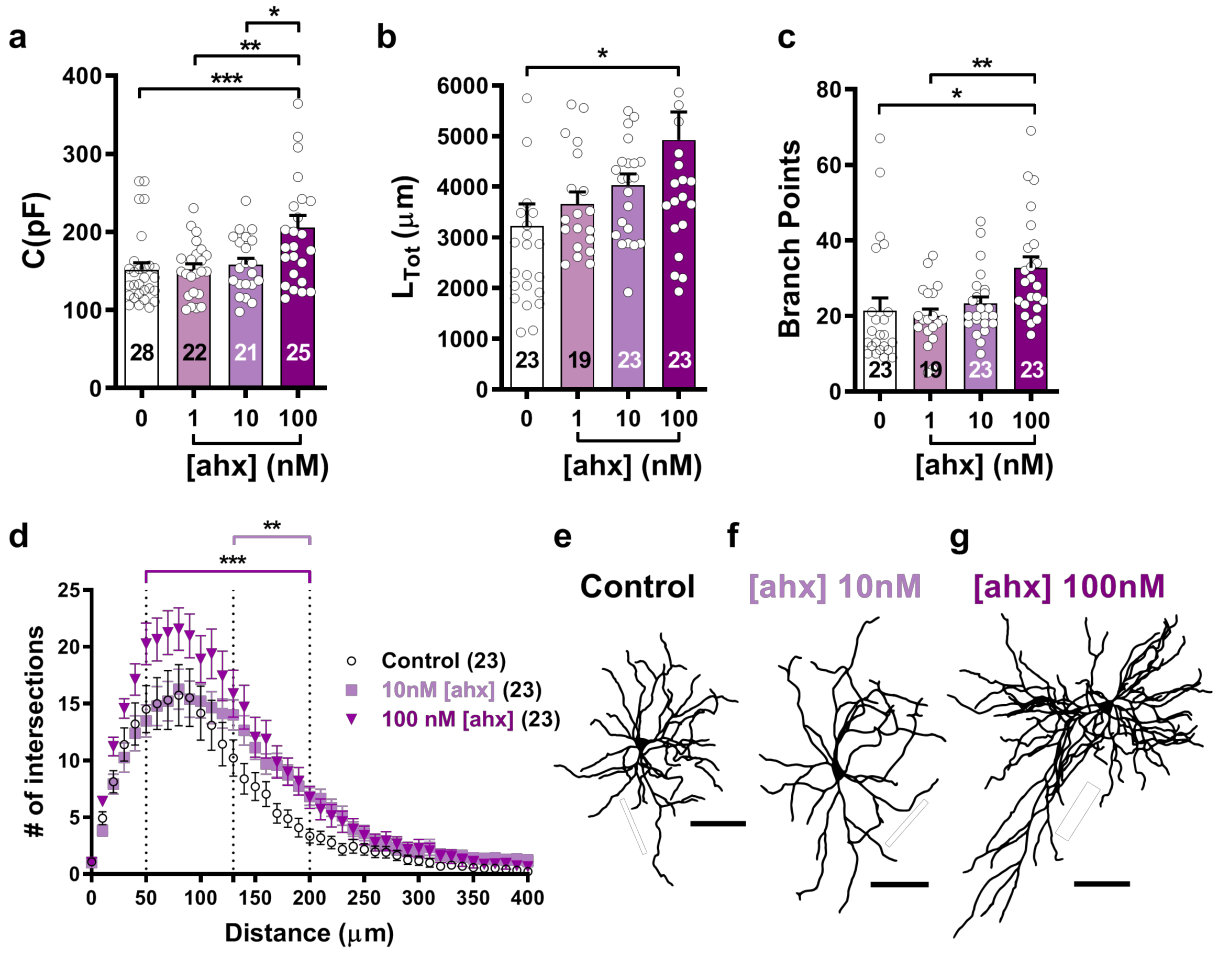

Figure 8._Treatment of BLA OTCs with the Y_2R agonist ahx causes pyramidal neuron hypertrophy. **a**. Scatter plot of mean capacitance of OTC pyramidal neurons treated with vehicle (n=26), ahx at 1 nM (n=23), 10 nM (n=21), and 100 nM (n=25) ($H_{(3)}$ = 11.31, p = 0.010). ***Inset*** Representative capacitative transients for control- or 10nM ahx-treated BLA OTC neurons. **b**. Scatter plot of mean total dendritic length for OTC neurons treated as in **a** ($H_{(3)}$ = 13.25, p = 0.0041). Vehicle (n=23), ahx at 1 nM (n=19), 10 nM (n=23), and 100 nM (n=23). **c.** Scatter plot of mean number of branch points in neurons in **b** ($H_{(3)}$ = 17.94, p = 0.0005). **d**. Sholl analysis of neurons in **b** and **c** treated as indicated (<u>Treatment:</u> $F_{(2, 66)}$ = 4.06, p = 0.022; <u>Distance:</u> $F_{(40, 2640)}$ = 119.5, p ~ 0;

309 Interaction: $F_{(80, 2640)} = 2.27$, $p = 1.92e^{-9}$; Purple = control vs 10 nM ahx; Black = control vs 100 nM
310 ahx). **e-g.** Representative reconstructions of neurons treated as indicated above. N-values for **c**
311 and **d** are as in **b**. For **a-c**, Kruskal-Wallis H tests with Dunn's post hoc tests. For **d**, 2-way RM ANOVA
312 with Tukey's post-hoc test. For **a-c**, circles represent neurons, black bars represent population
313 means, while in **d**, symbols represent population means and for all, error bars indicate s.e.m. All
314 tests were two-sided. *P<0.05, **P<0.01, ***P<0.001, ****P<0.0001 for post hoc multiple
315 comparisons. Scale bars in e-g = 100 µm

316 Finally, we tested the Y_5R-selective agonist, [cPP^{1-7},NPY^{19-23},Aib^{32},Gln^{34}] hPP (cPP)
317 (Cabrele et al., 2001) (1–100 nM). At 100 nM, cPP caused significant reductions in PN sEPSC
318 frequency and increased sIPSC frequency compared to controls, with no changes in sIPSC or sEPSC
319 amplitude (**Fig. 7d-g**). Concentrations of cPP ≥ 10 nM also caused robust decreases in PN whole-
320 cell capacitance (**Fig. 9a**), total dendritic length, and numbers of branch points (**Fig. 9b-g**). While
321 spine density was not altered by 100 nM cPP, estimates of total spine numbers per neuron were
322 significantly reduced when compared with vehicle controls (**Fig. 2**). Furthermore, co-incubation of
323 the Y_5R antagonist, CGP71683A (CGP, 30 nM) with a maximally effective concentration (30 nM)
324 of NPY not only prevented NPY effects on whole-cell capacitance and dendritic extent, but actually
325 caused dendritic hypertrophy (**Fig. 9a-g**). This effect is consistent with the Y_5 antagonist unmasking
326 the Y_2-mediated actions of NPY reported above.

327

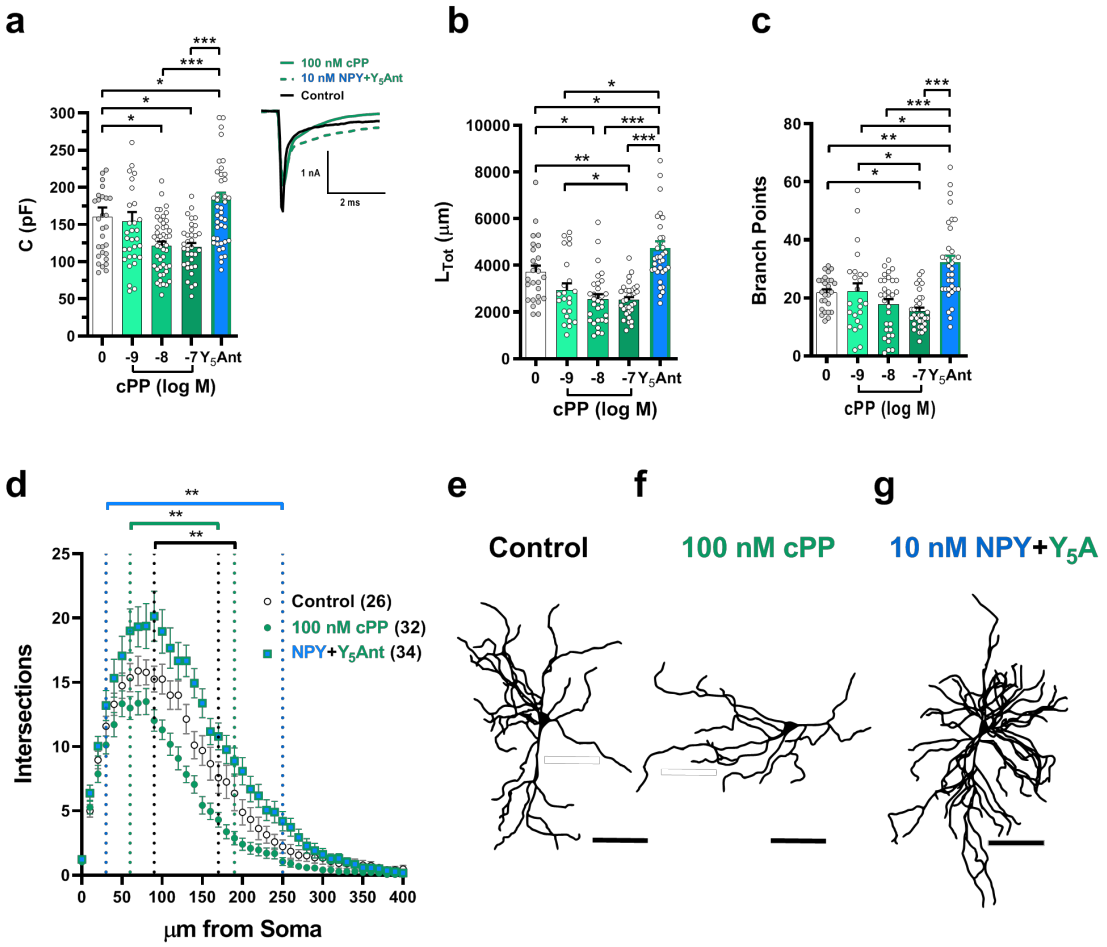

Figure 9. Treatment of BLA OTC with the Y_5R agonist cPP results in pyramidal neuron hypotrophy, which is blocked by the Y_5R antagonist CGP71683A (Y_5A). **a**. Scatter plot of mean capacitance of OTC pyramidal neurons treated with vehicle control (n=30), cPP at 1 nM (n=32), 10 nM (n=47) and 100 nM and 10 nM NPY with 30 nM CGP (n=45) ($H_{(4)}$ = 33.61, p = 8.97e^{-7}). ***Inset*** Representative capacitance transients from Control-, cPP- and NPY + Y_5Antagonist-treated BLA OTC neurons. **b**. Scatter plot of mean total dendritic length of neurons treated as in **a**. vehicle control (n=26), cPP at 1 nM (n=23), 10 nM (n=31) and 100 nM (n=32) and 10 nM NPY with 30 nM CGP (n=34) ($H_{(4)}$ = 49.88, p = 3.83e^{-10}). **c**. Mean number of branch points in neurons in **b** ($H_{(4)}$ = 36.99, p = 1.81e^{-7}). **d.** Sholl analysis for neurons in **b** and **c** treated as indicated (<u>Treatment:</u> $F_{(2, 90)}$ = 23.98, p = 4.49e^{-9}; <u>Distance:</u> $F_{(40, 3600)}$ = 175.1, p ~ 0; <u>Interaction:</u> $F_{(80, 3600)}$ = 3.91, p = 2.68e^{-28}). Black = control vs. 100 nM cPP; Green = control vs. NPY + Y_5A; Blue = 100 nM cPP vs. NPY + Y_5A. **e-g**. Representative traces from neurons treated as indicated. For **a-c**, Kruskal-Wallis H tests with Dunn's post hoc tests. For **d**, 2-way RM ANOVA with Tukey's post-hoc test. For **a-c**, circles represent neurons, black bars represent population means, while in **d**, symbols represent

344 population means and for all, error bars indicate s.e.m. All tests were two-sided. *P<0.05,
345 **P<0.01, ***P<0.001, ****P<0.0001 for post hoc multiple comparisons. Scale bars in e-g = 100
346 µm

347

348 ***In vivo* treatment of BLA with NPY or cPP results both in long-term behavioral stress**
349 **resilience and dendritic hypotrophy**

350 Based on the *in vitro* results, we hypothesized that NPY will cause similar effects on PN
351 structure in BLA *in vivo* that would also correlate with persistent increases in social interaction, a
352 measure of anxiety (File and Seth, 2003, Silveira et al, 2018), which permits repeated longitudinal
353 measures in individual animals, unlike many other paradigms such as the elevated plus maze. Five
354 sequential daily injections either of NPY (10 pmol/100 nL), the Y_1-agonist F^7P^{34}NPY (10 pmol/100
355 nL), the Y_5-agonist, cPP (10 pmol/100 nL), or NPY co-applied with the Y_5-antagonist CGP (each
356 10 pmol/100 nL) were given into bilateral BLA of 8 week-old male rats (Sajdyk et al., 2008). All
357 NPY agonist treatments in this experiment acutely increased social interaction (SI) on injection
358 days one and five relative both to pre-treatment baseline and to vehicle controls (**Fig. 10a**).
359 However, only animals treated with NPY or the Y_5-agonist retained this increase in SI at 2 and 4
360 weeks (**Fig. 10a**). In recordings from PNs in acute *ex vivo* BLA slices from these same animals at
361 4 weeks post-treatment, prior treatment with either NPY or the Y_5R agonist decreased whole-cell
362 capacitance (**Fig. 10b)** and significantly reduced dendritic extent and complexity relative to PNs
363 from the vehicle-treated animals (**Fig. 10c-j**). Co-administration of the Y_5R antagonist with NPY
364 prevented the long-term effects of NPY both on behavior and PN morphology (**Fig. 10a-e, j**); no
365 anxiogenic behavior was observed at any timepoint, nor were increases in PN capacitance or
366 arborization as seen in the OTCs. Therefore, the Y_5R is both necessary and sufficient to mediate

367 both the NPY-induced long term structural plasticity and decreased behavioral stress responses *in*

368 *vivo*.

369

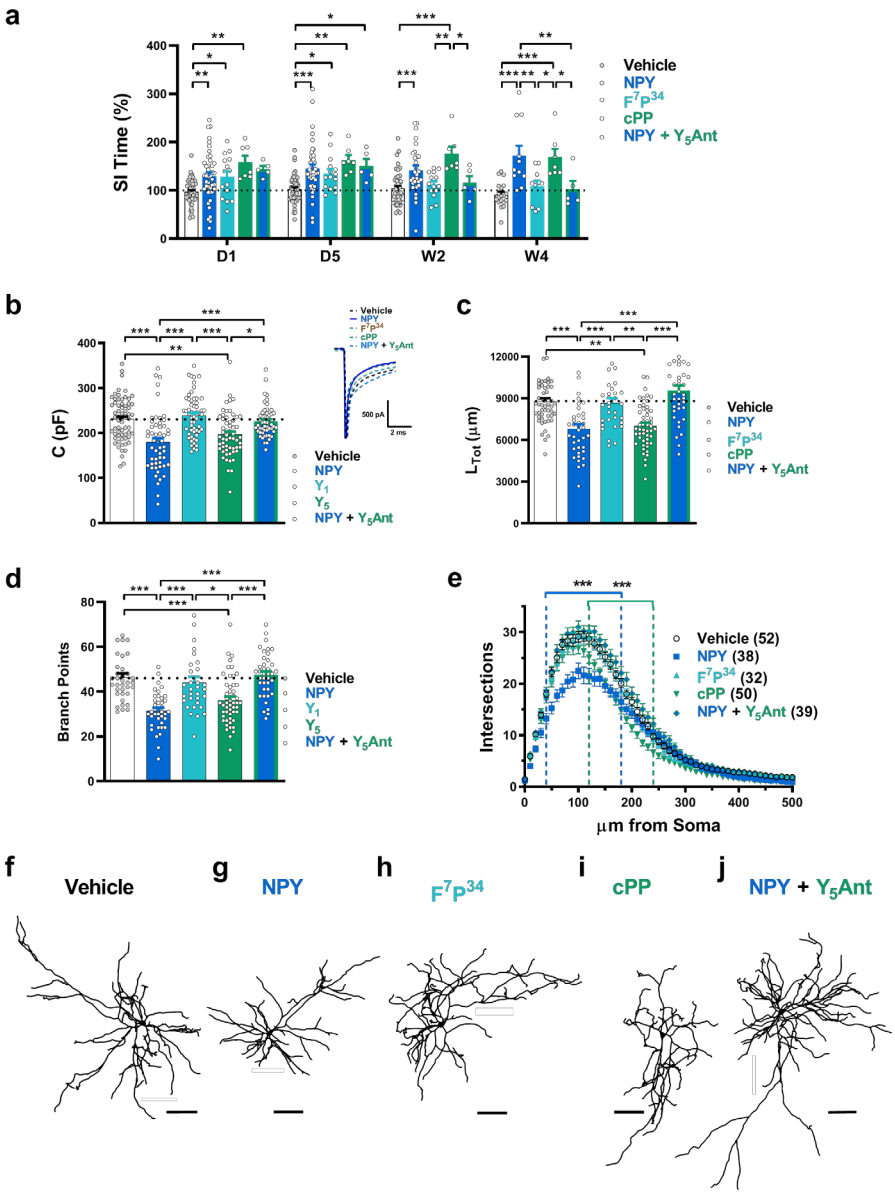

370 **Figure 10. Repeated *in vivo* injection of NPY or the Y_5 receptor agonist, but not the Y_1 receptor**
371 **agonist results in increased social interaction times and dendritic hypotrophy**. **a**. Scatter plot
372 depicting social interaction time shown as percent of individual animals' baselines for treatment
373 with vehicle control (100 nL) at day 1 (n=50), day 5 (n=49), week 2 (n=43) and week 4 (n=19); NPY
374 (10 pmol/100 nL) at day 1 (n=42), day 5 (n=40), week 2 (n=29) and week 4 (n=11); the Y_1 agonist

375 F^7P^{34}-NPY (10 pmol/100 nL) at day 1 (n=15), day 5 (n=14), week 2 (n=14) and week 4 (n=10); the
376 Y_5 agonist cPP (10 pmol/100 nL) at day 1 (n=7), day 5 (n=7), week 2 (n=7) and week 4 (n=7); and
377 NPY (10 pmol/100 nL) immediately preceded by the Y_5 receptor antagonist CGP71683A (Y_5A, 10
378 pmol/100 nL) at day 1 (n=5), day 5 (n=5), week 2 (n=5) and week 4 (n=5) (Linear Mixed-model;
379 Treatment: $F_{(4, 102.30)} = 14.11$, $p = 3.33e^{-9}$; Time: $F_{(3, 93.88)} = 1.66$, $p = 0.18$; Treatment * Time: $F_{(12,}$
380 $_{91.12)} = 1.87$, $p = 0.049$). **b**. Scatter plot of mean capacitance of BLA pyramidal neurons in acute
381 slices treated with vehicle control (n=64), NPY (n=53), F^7P^{34}-NPY (n=57), cPP (n=57) and NPY with
382 CGP (n=51) (Kruskal-Wallis H test with Dunn's post hoc test; $H_{(4)} = 47.74$, $p = 1.07e^{-9}$). **c**. Scatter
383 plot of mean total dendritic length for cells treated as in **b** (ANOVA with Tukey's post hoc; $F_{(4, 205)}$
384 $= 17.70$, $p = 1.70e^{-12}$). vehicle (n=52), NPY (n=38), F^7P^{34}-NPY (n=32), cPP (n=50) and NPY with CGP
385 (n=39). **d**. Scatter plot of mean number of branch points for neurons in **c** (Kruskal-Wallis H test
386 with Dunn's post hoc test; $H_{(4)} = 56.53$, $p = 1.55e^{-11}$). **e**. Sholl analysis for neurons in **c** and **d** as
387 indicated (2-way RM ANOVA with Tukey's post hoc test; <u>Treatment:</u> $F_{(4, 181)} = 13.09$, $p = 2.18e^{-9}$;
388 <u>Distance:</u> $F_{(49, 8869)} = 815.7$, $p = \sim 0$; <u>Interaction:</u> $F_{(196, 8869)} = 4.81$, $p = 1.23e^{-91}$). Blue = vehicle vs.
389 NPY; Green = vehicle vs. cPP. **f**-**j**. Representative traces from neurons treated as indicated above.
390 For **a**, symbols represent animals and black bars represent population means. For **b-d**, circles
391 represent neurons and black bars represent population means. For **e**, symbols represent
392 population means and for all, error bars indicate s.e.m. All tests were two-sided. **P*<0.05,
393 ***P*<0.01, ****P*<0.001, *****P*<0.0001 for post hoc multiple comparisons. Scale bars in f-j = 100
394 µm.

395

396 **Dendritic remodeling by NPY or CRF requires calcineurin or CaMKII, respectively**

397 Because the long term stress -vulnerability and -resilience effects of CRF and NPY are
398 mediated via CaMKII- and calcineurin, respectively in the BLA *in vivo* (Rainnie et al., 2004, Sajdyk
399 et al., 2008,), we hypothesized that the effects of NPY or CRF on BLA PN dendritic structure
400 require the actions of calcineurin or CaMKII activity, respectively. We first repeatedly incubated
401 BLA OTCs with NPY (10 nM) together with cyclosporin A (CsA, 2 µM), a protein phosphatase
402 (PP) inhibitor which blocks calcineurin (Liu et al, 1991). Addition of CsA inhibited NPY-mediated
403 dendritic hypotrophy and decreases in capacitance (**Fig. 11a-d**), resulting instead in PN dendritic
404 hypertrophy, possibly by unmasking a Y_2R activation (**Fig. 11b-d**). While these results are
405 consistent with a role for calcineurin, CsA is a general PP inhibitor and is not selective for
406 calcineurin (PP2b). Okadaic acid (OA) selectively inhibits both PP1 and PP2a but not calcineurin

407 (Cohen et al., 1990). Treatment of the BLA OTCs with the Y_5-agonist cPP (100 nM) in the presence

408 of OA (10 nM) did not alter the effects of the Y_5R agonist on either capacitance or dendritic

409 morphology, consistent with a specific role for calcineurin not only in NPY-mediated anxiolysis

410 (Sajdyk et al., 2008) but also in NPY-mediated PN dendritic hypotrophy (**Fig. 11a-d**).

411

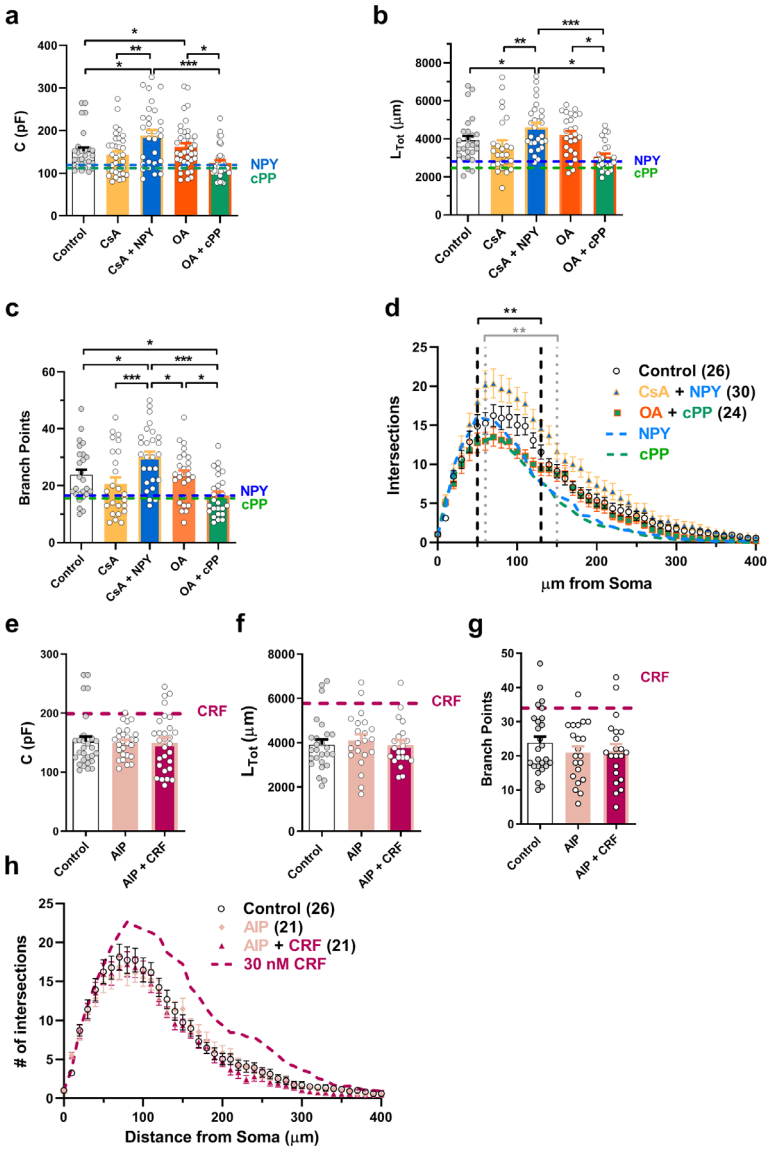

412 **Figure 11. Inhibitors of Calcineurin (CsA) and of CaMKII (AIP) respectively block NPY- and CRF-**
413 **mediated dendritic remodeling in BLA OTCs. a**. Scatter plot of mean capacitance of BLA OTC
414 pyramidal neurons treated with vehicle control (n=28) compared to CsA (2 nM) alone (n=35), CsA
415 (2 nM) and NPY (10 nM) (n=31), OA (10 nM) alone (n=39) and OA (10 nM) and cPP (10 nM) (n=38)
416 ($H_{(4)}$ = 22.80, p = 0.0001). Dashed lines represent mean for neurons treated with NPY (10 nM)
417 (blue) and cPP (100 nM) (green). **b**. Scatter plot of mean total dendritic length of pyramidal
418 neurons treated as in **a**, vehicle (n=26), CsA (n=26), CsA and NPY (n=30), OA (n=26) and OA and
419 cPP (n=24) ($H_{(4)}$ = 27.88, p = 1.32e^{-5}). **c.** Scatter plot of mean number of branch points for neurons
420 in **b** and **c,** with dashed lines representing the mean for neurons treated with NPY (blue) or cPP
421 (green) ($H_{(4)}$ = 28.93, p = 8.10e^{-6}). **d**. Sholl analysis for neurons in **b** treated as indicated, data for
422 neurons treated with NPY (blue) or cPP (green). Black = control vs. OA + cPP; Gray = control vs.
423 CsA + NPY (<u>Treatment:</u> $F_{(2, 78)}$ = 11.86, p = 3.18e^{-5}; <u>Distance:</u> $F_{(40, 3120)}$ = 150.0, p ~ 0.; <u>Interaction:</u>
424 $F_{(80, 3120)}$ = 2.39, p = 1.15e^{-10}). **e**. Scatter plot of mean capacitance values for BLA OTC pyramidal
425 cells treated with vehicle (n=28), AIP (40 nM) (n=27) and AIP (40 nM) and CRF (30 nM) (n=29), with
426 dashed line representing neurons treated with CRF ($H_{(2)}$ = 0.77, p = 0.68). **f**. Scatter plot of mean
427 total dendritic length for pyramidal cells treated as in **e** with neurons treated with CRF (dashed
428 line) ($H_{(2)}$ = 1.23, p = 0.54). Vehicle (n=26), AIP (n=21) and AIP and CRF (n=21). **g**. Scatter plot of
429 mean number of branch points in neurons in **f** with the mean for neurons treated with CRF (dashed
430 line) ($H_{(2)}$ = 0.81, p = 0.67). **h**. Sholl analysis for neurons in **f** and **g** treated as indicated compared
431 with neurons treated with CRF (dashed line) (<u>Treatment:</u> $F_{(2, 65)}$ = 0.50, p = 0.61; <u>Distance:</u> $F_{(40, 2600)}$
432 = 165.3, p ~ 0; <u>Interaction:</u> $F_{(80, 2600)}$ = 0.48, p = 0.99). For **a-c,e-g**, Kruskal-Wallis H tests with Dunn's
433 post hoc tests. For **d,h**, 2-way RM ANOVA with Tukey's post-hoc tests. For **a-c,e-g**, circles represent
434 neurons, black bars represent population means, while in **d,h**, symbols represent population
435 means and for all, error bars indicate s.e.m. All tests were two-sided. *P<0.05, **P<0.01,
436 ***P<0.001, ****P<0.0001 for post hoc multiple comparisons.

437

438 We then tested the role of CaMKII in mediating the hypertrophic actions of CRF in BLA
439 OTC PNs by using a cell-permeant CaMKII inhibitor, the myristoylated version of autocamtide-2-
440 related inhibitory peptide (AIP –Ishida et al., 1995). Inhibiting CaMKII activity with AIP (40 nM)
441 prevented the CRF-mediated (30 nM) increase in cell capacitance and dendritic hypertrophy (**Fig.**
442 **11e-h**). This is consistent with a role for CaMKII in CRF-mediated dendritic hypertrophy and the
443 resultant stress vulnerability generated by repeated stress and CRF treatment (Rainnie et al., 2004).

444
445 **DISCUSSION**
446

447 Unraveling mechanisms mediating adaptive and pathophysiological responses to stress is
448 key to developing treatments for stress-related disorders. The countervailing actions of CRF and
449 NPY on BLA PNs represent a suite of mechanisms contributing to adaptive stress responses in the
450 amygdala. Although both neuropeptides induce long-term neural changes linked to the initiation
451 or mitigation of stress responses, the mechanisms underlying the effects of these neuropeptides are
452 unclear. Here, we identify three novel and important insights into the function of NPY and CRF in
453 amygdala physiology. First, we found that NPY-induced stress resilience ultimately involves a
454 novel, persistent form of homeostatic plasticity, specifically, the reversible remodeling of dendritic
455 structure in BLA pyramidal output neurons mediated by the Y_5R, which counterbalances the
456 persistent hypertrophy seen with stress or repeated CRF exposure. Second, different NPY receptors
457 play nuanced and complex roles in the short-and long-term regulation of BLA excitability, structure
458 and behavior. Finally, the BLA OTC preparation is a robust *in vitro* model, that mimics and predicts
459 long-term *in vivo* responses of BLA neurons.

460 Chronic stress or UCN treatment causes dendritic hypertrophy and increases excitatory
461 inputs to BLA PNs (Padival et al., 2013, Rainnie et al., 2004); these increases in dendritic length
462 and spine number are associated with enhanced excitatory drive onto BLA PNs which increases
463 anxiety (Mitra et al., 2005, Padival et al., 2013, Adamec et al., 2012, Hill et al., 2011 Vyas et al.,
464 2002; 2006). Repeated intra-BLA administration of NPY *in vivo* decreases the overall excitability
465 of BLA PNs (Silveira Villarroel et al., 2018). Here we demonstrate similar effects of NPY on PNs
466 in BLA OTC, as well as its ability to reverse or constrain CRF's actions. Following repeated NPY
467 or CRF treatment, PNs in BLA OTCs also demonstrated respective decreases and increases in

468 sEPSC frequencies, consistent with their respective behavioral effects. NPY and CRF thus appear
469 to act via multiple, parallel mechanisms to mediate their opposing forms of plasticity, which when
470 combined, drive BLA PN structure toward a resting state similar to that of naïve BLA. Consistent
471 with a key role in stress homeostasis, NPY is thus poised to restore balance to the organism once a
472 threat has dissipated.

473

474 The predominant role of the Y_5R in driving the long-term effects on BLA physiology and
475 behavior was unanticipated. The Y_1R, which to date has received considerable attention in stress-
476 mitigation, contributes only to the acute actions of NPY on SI behavior and fear extinction
477 (Giesbrecht et al., 2010, Gutman et al., 2008). Because all NPY receptors couple to $G_{i/o}$ proteins
478 (Michel et al., 1998), the different roles played by these two receptors might result from independent
479 trafficking into separate signaling compartments within BLA neurons (Marley et al., 2013).
480 Moreover, while the Y_1R desensitizes in somatic cell lines (Berglund et al., 2003) and intact systems
481 (Holliday et al., 2005), evidence indicates that the Y_5R does not desensitize (Böhme et al., 2008).
482 This potentially significant difference suggests that the Y_5R is more likely to be available for lasting
483 mitigation of stress responses.

484

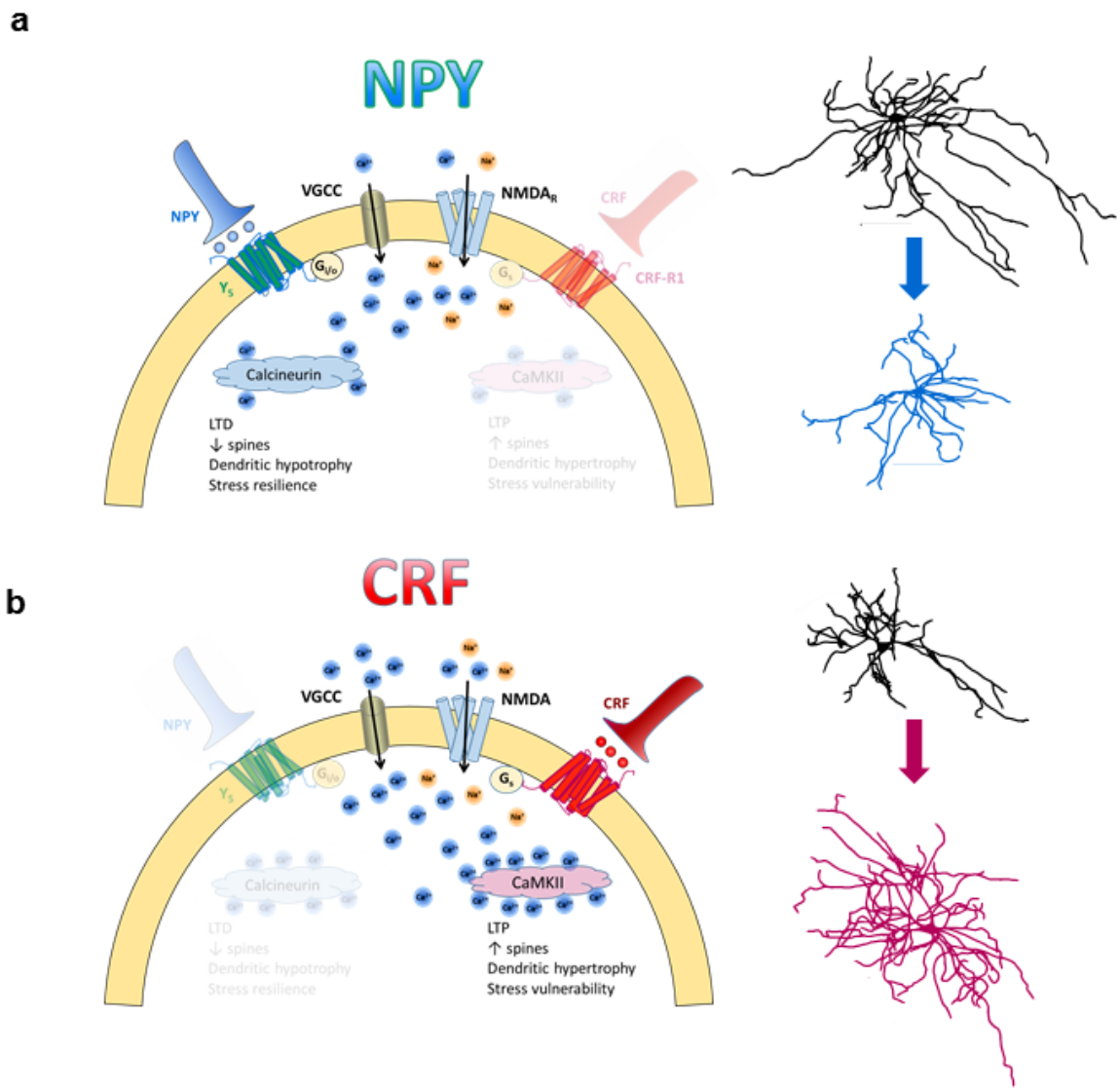

485

486 **Figure 12. Proposed model for the mechanism of action of NPY and CRF leading to dendritic**
487 **hypotrophy or hypertrophy respectively in BLA pyramidal cells. a.** NPY treatment results in net
488 activation of the Y_5R and PP2B (Calcineurin), resulting in a reduction in dendritic arborization
489 (illustrated right). **b.** CRF treatment results in net activation of CaMKII and hypertrophy of the
490 dendritic arbor. (Illustrated right).

491

492 The long-term effects of NPY or CRF require the respective activation of the Ca^{2+}-
493 dependent enzymes calcineurin and CaMKII, indicating a critical role for alterations in intracellular
494 Ca^{2+} levels in BLA PNs as demonstrated both *in vivo* (Sajdyk et al., 2008, Rainnie et al., 2004) and

495 now here in BLA OTCs. The acute and long-term enhancement of excitability caused by CRF
496 would result in robust elevations in intracellular Ca^{2+} ($[Ca^{2+}]_i$), consistent with CaMKII activation
497 requirements (Rainnie et al., 2004). However, how NPY achieves the more modest $[Ca^{2+}]_i$ elevation
498 needed by calcineurin is less obvious. In this context, the differential contributions of the multiple
499 NPY receptor subtypes within the BLA may provide some insight. Acute activation of BLA Y_2Rs
500 paradoxically results in anxiogenic behavioral responses (Sajdyk et al., 2004a; 2004b), and resulted
501 in CRF-like changes in BLA OTC neurons here. In both rat and mouse BLA, the Y_2R agonist
502 reduces tonic $GABA_B$R activation in BLA PNs by a presynaptically-mediated reduction in dendritic
503 GABA release. This causes an increase in dendritic excitability and a disinhibition of dendritic Ca^{2+}
504 channels, which in turn permits a moderately elevated Ca^{2+} influx in about half of BLA PNs
505 (Mackay et al., 2019). These effects suggest that NPY release in BLA activates all 3 NPY receptors:
506 Y_1Rs, which acutely hyperpolarize BLA PNs, Y_2Rs, which reduce dendritic $GABA_B$R activation
507 and Y_5Rs, whose long-term effects rely on the preferential activation of calcineurin. In this scenario,
508 the actions of the 3 separate NPY receptors would synergize to faciliate the Y_5R effect by modestly
509 elevating Ca^{2+} influx into BLA PNs (**Fig. 12a)** while preventing the larger increases in $[Ca^{2+}]_i$ that
510 would preferentially activate the CaMKII pathway favored by the CRF system (**Fig. 12b**). This
511 model could in part also explain the greater potency of the pan-agonist NPY to affect dendritic
512 structure. Nonetheless, further work is needed to more completely understand the pathways and
513 mechanisms involved in this long-term structural plasticity.

514 Regulation of cytosolic protein phosphorylation plays a key role in the structural plasticity
515 seen here, consistent with evidence that calcineurin and CaMKII act as downstream targets of
516 anxiolytic and anxiogenic molecules in the BLA (Rainnie et al., 2004, Mineur et al., 2014, Lin et
517 al., 2003). Both enzymes are inherently associated with synaptic plasticity in the BLA, so CRF- and

518 NPY-mediated alterations in dendritic structure might also engage mechanisms that underlie LTP
519 (long term potentiation) and LTD (long term depression), respectively (Pape and Pare, 2010). As
520 LTP and LTD each require different levels of $[Ca^{2+}]_i$, studies on intra-dendritic Ca^{2+} dynamics could
521 address the contributions made by acute or chronic changes in Ca^{2+} influx, either via NMDA
522 receptors (Rainnie et al., 2004) or voltage-dependent Ca^{2+} channels, to dendritic remodeling (Pape
523 and Pare, 2010).

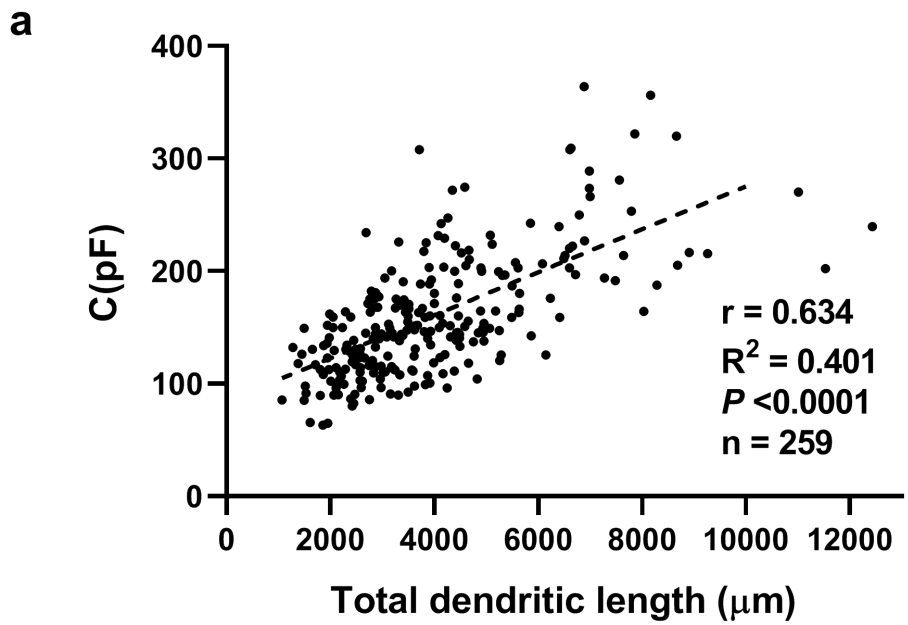

524

525 **Figure 13. Correlation between whole-cell capacitance and dendritic length. a.** Whole-cell
526 capacitance plotted against total dendritic length for 259 BLA OTC neurons from 100 different
527 OTCs taken from all experimental groups.

528 Total dendritic length and whole-cell capacitance were tightly correlated in BLA OTC PNs
529 over a variety of treatments (**Fig. 13**), were seen in BLA both *in vitro* and *in vivo*, and corresponded
530 with long-term behavioral changes. Despite the potent acute behavioral effects of Y_1R agonists,
531 they altered neither dendritic structure nor long-term behavior. It appears reasonable to speculate
532 that structural changes mediated by repeated peptide treatments result in the long-term changes in

533 behavioral response to stressors. In any case, this structural plasticity could provide a novel *in vitro*
534 bioassay predicting efficacy of drug candidates.

535 OTCs have proved useful in the study of longer-term nervous system changes such as
536 synaptic plasticity (Debanne et al., 1999, Selcher et al., 2012), and those associated with pathologies
537 such as chronic pain (Lu et al., 2006), or even prion disorders (Campeau et al., 2013). Since such
538 changes can involve alterations not only in synaptic microanatomy but also more robust changes in
539 cellular architecture, the preservation of anatomical relations within the OTC is a distinct advantage.
540 Mature PNs in BLA OTCs share more electrophysiological attributes with those in age-matched
541 (10W) *ex vivo* BLA than those in *ex vivo* P14 rats, despite their increased compactness compared
542 with neurons from either *ex vivo* preparation. Capacitance values were smaller, I_h activation
543 kinetics (tau_{fast} and tau_{slow}) were faster, and sEPSC and sIPSC amplitudes were larger in BLA OTCs
544 compared with the acute *ex vivo* neurons **(Table 1**). However, the properties of BLA OTC PNs as
545 indicated by action potential properties, firing rates and AHPs suggests that growth within OTCs
546 constrains the physical extent of otherwise physiologically mature OTC neurons.

547

	Acute P14	Acute 10W	OTC EP 10W	ANOVA
RMP (mV)	-76.8 ± 0.5 *** n=56	-81.3 ± 0.7 n=44	-77.9 ± 1.0** n=54	F(2, 151) = 9.05, p= 0.0002
Rheobase (pA)	126.3 ± 5.2 **** n=56	309.2 ± 13.8 n=44	248.2 ± 24.8*, #### n=54	F(2, 151) = 29.84, p = 0.00019
I_R (MΩ)	176.8 ± 6.4 **** n=56	71.5 ± 5.2 n=22	103.4 ± 6.3*, #### n=49	F(2, 124) = 64.16, p = 7.43e-20
I_h max (pA)	-175.2 ± 7.3*** n=52	-362.5 ± 25.9 n=48	-290.4 ± 20.1*, ### n=49	F(2, 146) = 25.09, P = 4.31e-10
I_h density (pA/pF)	-0.96 ± 0.03 * n=52	-1.36 ± 0.10 n=22	-1.64 ± 0.13 #### n=49	F(2, 120) = 14.38, p=2.52e-6
C_m (pF)	180.2 ± 3.7 **** N=56	230.6 ± 7.3 N=44	150.0 ± 5.8 ****, ### N=58	F(2, 155) = 49.98 P=1.75e-18,
sIPSC AMP (pA)	25.5 ± 1.1 n=25	24.13 ± 1.8 n=25	49.8 ± 4.9 ****, #### n=25	F(2, 72) = 21.59, p=4.51e-8

sIPSC IEI (ms)	2249 ± 417 **** n=25	213.9 ± 22.1 n=25	155.6 ± 19.3 #### n=25	F(2, 72) = 24.41 p= 8.07e-9
sEPSC AMP (pA)	25.9 ± 0.9 n=25	26.87 ± 2.3 n=25	44.8 ± 2.1 ****, #### n=25	F(2, 72) = 32.15 p = 1.05e-10
sEPSC IEI (ms)	1241 ± 347.2 ** n=25	171.1 ± 26.4 n=25	221.5 ± 32.2 ## n=25	F(2, 72) = 8.95 p=0.0003
Total Dendritic Length (µm)	5986 ± 337 **** n=17	8644 ± 284 n=36	3625 ± 187.4****, ####, n=39	F(2, 89) = 113.6 p = 3.16e-25
# of branches	37.5 ± 2.3 * n=17	46.3 ± 1.9 n=36	20.5 ± 1.5 ****, #### n=39	F(2, 89) = 60.17 p = 2.95e-17

Table 1. Comparison of electrophysiological and morphological properties of acute P14, acute 10W and EP 10W OTC pyramidal neurons in the BLA.

Data presented as mean ± s.e.m. One-way ANOVA with Tukey's post-hoc test for multiple comparisons were used for all analyses; *P<0.05, **P<0.01, ***P<0.001, ****P<0.0001 vs Acute 10W, #P<0.05, ##P<0.01, ###P<0.001, ####P<0.0001 vs Acute P14 for multiple comparisons.

In summary, we report a novel, readily and completely reversible alteration in PN dendritic structure that accompanies the long-term increase in behavioral stress resilience caused by NPY in the BLA, the mirror opposite of equivalent CRF actions. These robust changes are readily observed in BLA OTCs, and are reflected nearly perfectly *in vivo*. The acute and longer-term actions both of NPY and CRF involve regulation of the same elements (I_h, dendrites) in the PN, changes that correlate with alterations in excitability. The coordinated, countervailing regulation of these PN properties by NPY and CRF suggests other signals could access this machinery to regulate stress responses mediated by the BLA.

MATERIALS AND METHODS

Animals

All animal procedures were approved by the University of Alberta Animal Care and Use Committee: Health Sciences, in accordance with the guidelines of the Canadian Council on Animal

567 Care. Litters of postnatal day (P) 14 and 5-week old male Sprague-Dawley rats were used. P14
568 pups were given complete access to the dams for maternal care; then were removed from the dam
569 just prior either to preparation of OTCs or for a subset of acute slice studies. Five week old rats
570 were grouped housed (2-3 animals per cage) with 12:12 hours light:dark schedule and *ad libitum*
571 access to food and water.

572 **Development and validation of organotypic slice cultures (OTCs) of BLA**

573 Postnatal development of the rat BLA continues until P28 (Ehrlich et al., 2012; 2013).
574 Generation of OTCs from late adolescent or early adult-stage animals would be ideal, but the
575 viability of OTCs declines steeply with postnatal age of origin (Humpel, 2015, Kim et al,, 2013).
576 Our and others' previous work used larger (250 - 275g) Wistar or older (P42) Sprague-Dawley rats
577 in studies of NPY and UCN effects on stress-resilience/vulnerability (Molosh et al., 2013), and
578 acute and persistent NPY actions (Giesbrecht et al., 2010, Silveira Villarroel et al., 2018).

579 **OTC preparation**

580 Organotypic cultures were prepared using the interface method described by Stoppini et al.
581 (1991) with minor modifications. Briefly, P14 rats were decapitated and their brains rapidly
582 removed under sterile conditions and submerged in ice-cold slicing solution [Hank's balanced salt
583 solution (HBSS) + D-glucose (0.6% final) + kynurenic acid (30 μM final)]. The brain was imbedded
584 in agarose and trimmed agarose-brain blocks were secured with cyanoacrylate glue to a custom
585 slicing chamber, immersed in cold (<4ºC) slicing solution. Coronal slices (350 μm) were cut serially
586 from rostral to caudal using a vibratome and trimmed to size. Four slices per hemisphere containing
587 the BLA (as determined visually with a dissecting microscope), were allowed to rest in fresh slicing
588 solution at 4°C for 30-45 minutes, and mounted on individual semiporous membrane inserts and

589 placed in 24-well plates with 300 μL of culture media (50% Minimal Essential Medium (MEM),
590 25% heat-inactivated horse serum, 25% HBSS, supplemented with: 1 mM Glutamax, 1% D-
591 glucose, 0.5 mM L-ascorbic acid, and 25 U/mL penicillin/streptomycin). After 48 hours in culture,
592 an anti-mitotic solution of 1:1:1 cytosine-β-D-arabino-funanoside, uridine, and 5-Fluro-2'-
593 deoxyuridine was added to the media (0.5 μM final concentration) for 24 hours to prevent glial
594 proliferation. Slices were maintained at 37°C in 5%/95% CO_2/air. Media was changed three times
595 per week for the duration of the experiment, except as indicated.

596 BLA OTCs prepared from rats at P21 and P28 were poorly viable, but those from P14 (2
597 week) rats remained robustly viable to at least 8 weeks in culture, the equivalent postnatal (EP) age
598 of P70 (**Fig. 3a**), permitting comparison of the electrophysiological and morphological properties
599 of PNs from the OTCs (see below). Such OTCs were used for this entire study

600 **OTC drug incubations**

601 To mimic EP 6 weeks (4 weeks in culture), slices were treated with fresh media containing
602 indicated concentrations of reagents, changed daily for five consecutive days; the last change
603 remained until the normal Day 7 media change. When cultures were serially treated as above first
604 with NPY then with CRF (or vice-versa), incubations proceeded with one peptide as above,
605 followed with an identical one-week daily protocol using the opposing peptide starting with the
606 Day 7 media change. A control subset of cultures was treated with the inactive desamido NPY
607 analogue (daNPY – 100 nM). After incubations, media changes were again performed three times
608 weekly (**Fig. 3a**).

609 **Acute slice preparation**

610 P14 or P70 rats were decapitated and their brains rapidly submerged in cold (4°C) artificial
611 cerebrospinal fluid (aCSF) slicing solution, containing (in mM): 118 NaCl, 3 KCl, 1.3 $MgSO_4$, 1.4
612 NaH_2PO_4, 5.0 $MgCl_2$, 10 D-glucose, 26 $NaHCO_3$, 2.5 $CaCl_2$ and 1.0 kynurenic acid and bubbled
613 with carbogen (95% O2, 5% CO_2) (Silveira Villarroel et al., 2018). Coronal sections (300 µm)
614 containing the BLA were prepared using a vibrating slicer (HR2; Sigmann Elektronik, Hüffenhardt,
615 Germany). Brain slices were then transferred to a room temperature (22°C), carbogenated aCSF
616 containing the following (in mM): 124 NaCl, 3 KCl, 1.3 $MgSO_4$, 1.4 NaH_2PO_4, 10 D-glucose, 26
617 $NaHCO_3$, and 2.5 $CaCl_2$. Osmolality was adjusted to 300 mOsm/kg.

618 **Comparison with PNs from acute slice preparations**

619 PNs from BLA OTCs are morphologically complex and electrophysiologically more similar to
620 PNs in acute slices from P70 than from P14 rats, though OTC neurons are considerably smaller
621 than those from either acutely ex vivo (**Table 1**). Moreover, repeated NPY (100 nM) treatment of
622 OTCs *in vitro* (**Fig. 3a)** increased the mean amplitude of spontaneous inhibitory postsynaptic
623 currents (sIPSCs), while increasing the mean inter-event interval (IEI) of spontaneous excitatory
624 postsynaptic currents (sEPSCs). In all, repeated NPY treatment resulted in similar a net increase
625 in synaptic inhibition and reduction of synaptic excitation onto BLA PNs in OTCs as *in vivo* (**Fig.**
626 **3b-e**).**Stereotaxic surgery and intracranial injections.**

627 Stereotaxic surgery was carried out as described in detail elsewhere (Silveira Villarroel et
628 al., 2018). Briefly, 5-week old animals were acclimatized to the animal facility and handled daily
629 for 1 week prior to experimental manipulation. Rats were anesthetized with ketamine/xylazine
630 (90:10 mg/kg) or with isoflurane using a SomnoSuite low flow vaporizer (Kent Scientific,
631 Torrington, CT, USA) and placed in a stereotaxic apparatus (Kopf, Tujunga, CA, USA).
632 Anaesthesia was monitored carefully to maintain surgical plane throughout, and animals were kept
633 warm with a temperature-controlled blanket (Harvard Apparatus, Holliston MA, USA). Bilateral
634 guide cannulas (26 gauge; Plastics One, Roanoke, VA, USA) were implanted to just above (2 mm)

635 the BLA [anteroposterior (AP): -2.3; mediolateral (ML): ±5.0; dorsoventral (DV): -6.4; incisor bar:
636 -3.2 mm] (Paxinos and Watson, 1986). The cannulas were secured to the skull with four stainless
637 steel screws (2.8 mm; Plastics One, Roanoke, VA, USA) and self-curing acrylic resin (Lang Dental
638 Manufacturing Company, Inc., IN, USA). After completion of surgery, all animals received
639 meloxicam (Boerhringer Ingelheim, Burlington, Ontario, Canada; 1 mg/kg, s.c.), 1 ml of saline
640 0.9% s.c., and were placed in a warm environment until they had fully recovered from the
641 anesthetic. Rats remained singly housed until they fully recovered from surgery, then were housed
642 in pairs. Pairs were separated and animals housed singly one day prior to behavioral testing (below).

643 **Intracranial injections**

644 As reported elsewhere (Silveira Villarroel et al., 2018), all compounds were delivered
645 bilaterally via 33 gauge injection cannulas (Plastics One) that extended 2 mm beyond the guide
646 cannulas, using a dual-channel infusion pump (PHD ULTRA, Harvard Apparatus, Holliston, MA,
647 USA). Vehicle (sterile saline) alone or containing drug(s) as described was delivered at 100 nL/30s
648 per side; cannulae were left in place for 1 minute afterward to prevent backflow. All injections were
649 performed once daily between 8:00 AM and 10:00 AM for successive 5 days. Animals rested in
650 their home cage for 30 min following injections, then tested (if in their protocol) for social
651 interaction (SI).

652 **Behavioral testing**

653 The SI test was performed according to Sajdyk et al., (2008), with minor modifications. Briefly,
654 an experimental animal was placed into the SI box (96 cm long x 96 cm wide x 30 cm high with
655 an open top) simultaneous with a partner rat of the same sex, age and weight, housed under
656 identical conditions but which had not encountered the experimental animal previously. Seventy-

657 two hours after implantation surgery, rats were given a sham injection, then allowed to spend 10
658 minutes alone in the arena to acclimate. Twenty-four hours later they received another mock
659 injection, and SI was tested to establish baseline anxiety-like levels prior to any experimental
660 manipulations. Two days later, rats received a bilateral intra-BLA injection (vehicle or drug) and
661 were tested for SI 30 min later (day 1). Injections continued daily at the same time and the SI test
662 was repeated 30 min after the fifth injection (day 5), then at 2 weeks and 4 weeks from the first
663 injection. Behavior was video recorded and later analysed by individuals blinded to treatment.

664 **Whole-cell patch clamp electrophysiology**

665 Acutely prepared slices or EP 9-10 week OTC slices (with culture insert membrane still
666 attached), were transferred to a fixed recording chamber beneath a movable upright microscope
667 (Axioskop FS2; Carl Zeiss, Germany)(Giesbrecht et al., 2010, Silveira Villarroel et al., 2018).
668 Slices were perfused at 2-3 mL/min for at least 10 minutes before recording, with warmed (32-
669 34°C), carbogenated aSCF (300 mOsm/L acute slices and 320 mOsm/L for OTCs - adjusted with
670 NaCl). Patch pipettes were pulled from borosilicate glass (TW150F; World Precision Instruments,
671 Sarasota, FL, USA) with a two-stage puller (PP-83; Narishige, East Meadow, NY, USA) and had a
672 resistance of 4-6 MΩ with an internal solution (mM): 126 K-gluconate, 4 KCl, 10 HEPES, 5
673 MgATP, 0.3 NaGTP, 1 EGTA, 0.3 $CaCl_2$ and 0.2% neurobiotin (pH 7.27, 275 mOsm/L for acute
674 slices and 300 mOsm/L for OTCs).

675 The BLA was identified under a 5x objective and PNs identified visually with infrared-
676 differential interference contrast (60x) optics. Neurons were selected as previously reported
677 (Giesbrecht et al., 2010, Silveira Villarroel et al., 2018) based on morphological and
678 electrophysiological criteria. PNs chosen for study were in random locations throughout the BLA;

679 1-3 neurons per slice were studied. Either a Multiclamp 700B or AxoClamp2A amplifier was used
680 together with a DigiData 1322 or Digidata 1440 interface and pCLAMP v10.4 software (all
681 Molecular Devices, Sunnyvale CA, USA). Gigohm seal, whole-cell recordings were low-pass
682 filtered at 2 kHz and digitized at 10 kHz. Access resistance was measured throughout the
683 experiment, and only those cells with changes less than 20% were kept for further analysis. The
684 membrane potential reported was corrected offline for the calculated 15 mV liquid junction
685 potential (Silveira Villarroel et al., 2018, Chee et al., 2010). Recordings (> 20 min) were terminated
686 by gradually withdrawing the pipette until the membrane re-sealed.

687 Capacitance was calculated offline with pClamp, from the area under the curve of the current
688 amplitude from a 200 ms, 10 mV hyperpolarizing voltage step (Taylor, 2012). No capacitance
689 compensation was applied during these measurements. Spontaneous synaptic activity was assessed
690 in voltage clamp at a (corrected) holding potential of -55 mV and sampled at 20 kHz.

691 **Cell processing and labeling**

692 Neurons from *ex vivo* and OTC slices were all processed, stained, imaged, reconstructed
693 and subjected to the same morphological analyses. Following patch clamp recordings, OTCs and
694 acute slices were fixed with 10 % formalin (Thermo Fisher Scientific, Ottawa, Ontario, Canada) for
695 24-72 h at 4°C, and then transferred to 0.2% sodium azide in PBS for subsequent storage at 4 °C.
696 Slices were processed within 4 weeks following patch clamp recordings. Free-floating slices were
697 washed for 3 x 10 min periods in PBS before blocking and permeabilization for 2 h with 0.3 %
698 Triton X-100 in PBS and 4% normal goat serum (Sigma-Aldrich, Oakville, Ontario, Canada). Slices
699 were incubated with streptavidin conjugated with Alexa Fluor 555 or 546 (1:1000; Life
700 Technologies, Grand Island, New York, USA) in 0.3 % Triton X-100 in PBS with 4% normal goat

701 serum for 3 h at room temperature. Slices were washed 4 x10 min each in PBS, mounted on
702 Superfrost Plus slides and coverslips were applied with Prolong Gold mounting media (Thermo
703 Fisher). Slides were allowed to air dry in the dark at room temperature before being imaged via
704 confocal microscopy.

705 **Imaging and neuronal reconstruction**

706 For morphological analysis of filled neurons, z-stack images were obtained with a 20x
707 objective, 1024 x 1024 resolution, 100 Hz, excitation wavelength 543 nm, for a series of 0.8 µm
708 steps with a laser scanning confocal microscope (Leica TCS SP5; Leica Microsystems, Canada).
709 To determine the position of each neuron within the slice, multiple single-plane images were taken
710 at 10x magnification, 512 x 512 resolution and 100 Hz, and stitched together using Leica LAS AF
711 software. Only those neurons whose dendritic arbor was clearly and completely filled and cell body
712 was clearly within the boundaries of the BLA were used for analysis. Neuronal reconstruction was
713 performed using the simple neurite tracer function in FIJI (NIH, Bethesda, MD, USA). Following
714 tracing, Sholl analysis (Sholl, 1953) of the entire 3-dimensional dendritic arbor was performed with
715 another FIJI software module using concentric circles with increasing radii of 10 µm to determine
716 dendritic intersections vs. distance from the soma. Total dendritic length and dendritic branching
717 was calculated using FIJI and Excel software. Quantification of dendritic spine density was
718 achieved by manually counting dendritic spines in z-stack images taken at 100x magnification, 1024
719 x 1024 resolution and 100 Hz for a series of 0.5 um steps. Spines were counted on three separate,
720 randomly selected, 100 µm dendrite segments for each neuron analysed in a treatment group. All
721 protrusions that were connected to the dendrite segment were considered as spines, but were not
722 categorized by spine morphologies. Total spine number was estimated from the average spine

723 density and total dendritic length for an individual neuron. Experimenters were blinded to culture
724 treatment at the time of reconstructions.

725 **Reagents and Drugs**

726 NPY (human, rat) was purchased from Polypeptide Group (San Diego, CA, USA) while
727 CRF was obtained from Phoenix Pharmaceuticals Inc. (Burlingame, CA, USA). The Y_1-agonist
728 (F^7,P^{34}-NPY), the Y_5-agonist ([cPP^{1-7},NPY^{19-32},Ala^{31},Aib^{32},Gln^{34}]hPP) and the Y_2 agonist ([ahx^{5-}
729 ^{24}] NPY) were generous gifts from Dr. A.G. Beck-Sickinger (Leipzig, Germany), while the Y_5-
730 antagonist, CGP71683, was purchased from Tocris Bioscience (Bristol, UK). Cyclosporine A and
731 okadaic acid were gifts from Drs. Shairaz Baksh and Charles Holmes (University of Alberta,
732 Canada). The cell permeable CaMKII inhibitor, myristoylated-autocamtide-2- related inhibitory
733 peptide, was obtained from Enzo Life Sciences, Inc (Farmingdale, NY, USA). Culture reagents
734 were all obtained from Gibco, except for Cytosine–β-D-arabino-furanoside, Uridine and 5'Fluro-
735 2'deoxyuridine, which were from Sigma-Aldrich Canada. Pipette solution reagents were all from
736 Sigma-Aldrich, except for Na-GTP (Roche Diagnostics).

737 **Data analysis and statistics**

738 Electrophysiological recordings were viewed offline using pCLAMP. Traces from
739 electrophysiological recordings, statistical analysis and graphs were prepared using versions 5 – 8
740 of Prism software (GraphPad, San Diego, CA, USA) or SPSS (version 20 - IBM). Neuronal
741 reconstruction and Sholl analysis was performed using modules of the FIJI software suite (National
742 Institutes of Health). Unless otherwise stated, all data are represented as mean ± s.e.m. D'Agostino-
743 Pearson omnibus normality test was applied to determine data distributions. One-way analysis of
744 variance (ANOVA) with Tukey's post-hoc test or Kruskal-Wallis H tests with Dunn's post hoc test

745 were used as indicated, to compare cell capacitance, total dendritic lengths, branch points and spine
746 density/total spine estimates between treatments. For Sholl analysis, two-way repeated measures
747 ANOVA were used with Tukey's post-hoc test for multiple comparisons. A Linear Mixed-Model
748 was used for analysis of SI studies. Treatment and time (with interaction term) were used as fixed
749 effects, while we used intercepts for subjects as random effects. For data in **Table 1**, one-way
750 ANOVA with Tukey's post-hoc test for multiple comparisons was used. For sEPSC and sIPSC
751 analyses, two-sided Student's t-test or Mann-Whitney U tests were performed when applicable.
752 OTC cultures for any given experiment were obtained from at least 3 animals (typically more), with
753 data acquired from 1-3 neurons per OTC. With the extent of time in culture, and minimal number
754 of neurons recorded from per slice, we opted to treat each neuron as an independent observation for
755 statistical analysis. The number of animals, cultures and neurons per experimental group are
756 indicated in **Table 2**. No statistical test was used to predetermine sample sizes, but our sample sizes
757 are similar to those previously reported in the field (Adamec et al., 2012, Silveira Villarroel et al.,
758 2018, DeSimoni et al., 2003). All analyses were two-sided. Significance was set at $P<0.05$ (*
759 $P<0.05$, **$P<0.01$, ***$P<0.001$, ****$P<0.0001$).

760

761 **Acknowledgments:** We are grateful for the generous contributions of NPY receptor-selective
762 agonists by Prof. Annette Beck-Sickinger, University of Leipzig. SDM received funding from
763 Alberta Innovates Health Solutions (AIHS) (Doctoral studentship). JPM received Canadian
764 Institute of Health Research (CIHR) (Doctoral and Masters studentships), and a Doctoral
765 studentship from AIHS. WFC was a Medical Scientist of the Alberta Heritage Foundation for
766 Medical Research for most of this period.
767 This work was supported by NIH grants MH081152 and MH090297 (to JHU & WFC), and
768 support by the University of Alberta Hospitals Foundation to WFC.
769 **Author Contributions:** . SDM, APMT, JHU and WFC designed experiments. SDM, APMT,
770 AM, HSV and JM performed experiments. SDM, APMT and AM analyzed data. SDM, JHU and
771 WFC wrote the manuscript. SDM and WFC conceived the study. All authors edited the
772 manuscript.
773 **Competing Interests:** The authors declare no competing financial interests.
774

775 **Data availability:** The data that support the findings of this study are available from the
776 corresponding author upon reasonable request.

777

Electrophysiological Figures					Morphology Figures				
Figure	**Treatment**	**Neurons**	**Cultures**	**Animals**	**Figure**	**Treatment**	**Neurons**	**Cultures**	**Animals**
1a	Control	42	20	18	1b-d	Control	26	19	16
1a	NPY ($1e^{-10}$ M)	31	15	3	1b-d	NPY ($1e^{-10}$ M)	26	14	3
1a	NPY ($1e^{-9}$ M)	43	25	23	1b-d	NPY ($1e^{-9}$ M)	25	16	15
1a	NPY ($1e^{-8}$ M)	47	27	20	1b-d	NPY ($1e^{-8}$ M)	21	16	14
1a	NPY ($1e^{-7}$ M)	49	26	21	1b-d	NPY ($1e^{-7}$ M)	24	16	13
1a	da-NPY ($1e^{-7}$ M)	30	14	13	1b-d	da-NPY ($1e^{-7}$ M)	20	12	11
3d,e	Control	25	11	5	2d,e	Control	15	11	6
3d,e	NPY ($1e^{-7}$ M)	25	13	7	2d,e	NPY ($1e^{-7}$ M)	15	10	6
3h	Control	25	14	8	2d,e	CRF ($3e^{-8}$ M)	15	10	5
3h	CRF ($3e^{-8}$ M)	25	16	9	2d,e	cPP ($1e^{-7}$ M)	15	8	5
4a	Control	39	19	14	4b-d	Control	33	19	14
4a	CRF ($3e^{-10}$ M)	40	21	11	4b-d	CRF ($3e^{-10}$ M)	31	19	11
4a	CRF ($3e^{-9}$ M)	36	18	11	4b-d	CRF ($3e^{-9}$ M)	26	15	11
4a	CRF ($3e^{-8}$ M)	38	20	11	4b-d	CRF ($3e^{-8}$ M)	28	18	10
5a	Control	42	24	21	5b-d	Control	26	21	16
5a	CRF-NPY	31	15	6	5b-d	CRF-NPY	23	13	6
5a	NPY-CRF	32	15	7	5b-d	NPY-CRF	23	12	6
5h	CRF-NPY	25	12	5	6b-d	Control	27	15	13
5h	NPY-CRF	25	10	4	6b-d	F^7P^{34}-NPY ($1e^{-9}$ M)	19	14	12
6a	Control	30	22	19	6b-d	F^7P^{34}-NPY ($1e^{-8}$ M)	18	15	10
6a	F^7P^{34}-NPY (1^{e-9} M)	28	19	15	6b-d	F^7P^{34}-NPY ($1e^{-7}$ M)	22	14	13
6a	F^7P^{34}-NPY ($1e^{-8}$ M)	34	20	14	8b-d	Control	23	11	9
6a	F^7P^{34}-NPY ($1e^{-7}$ M)	34	22	18	8b-d	ahx ($1e^{-9}$ M)	19	11	10
7c	Control	25	15	9	8b-d	ahx ($1e^{-8}$ M)	23	15	13
7c	F^7P^{34}-NPY ($1e^{-7}$ M)	25	18	13	8b-d	ahx ($1e^{-7}$ M)	23	13	10
7f,g	Control	25	15	9	9b-d	Control	26	17	13
7f,g	cPP ($1e^{-7}$ M)	25	14	8	9b-d	cPP ($1e^{-9}$ M)	23	17	11
8a	Control	26	12	9	9b-d	cPP ($1e^{-8}$ M)	31	17	12
8a	ahx ($1e^{-9}$ M)	23	10	8	9b-d	cPP ($1e^{-7}$ M)	32	17	13
8a	ahx ($1e^{-8}$ M)	21	12	8	9b-d	NPY ($1e^{-8}$ M) + CGP (3^{e-8} M)	34	17	5
8a	ahx ($1e^{-7}$ M)	25	14	10	11b-d	Control	26	17	4
9a	Control	30	20	13	11b-d	CsA ($2e^{-9}$ M)	26	14	4
9a	cPP ($1e^{-9}$ M)	32	18	12	11b-d	CsA ($2e^{-9}$ M) + NPY ($1e^{-8}$ M)	30	17	4
9a	cPP ($1e^{-8}$ M)	47	26	16	11b-d	OA ($1e^{-8}$ M)	26	12	4
9a	cPP ($1e^{-7}$ M)	34	23	15	11b-d	OA ($1e^{-8}$ M) + cPP ($1e^{-7}$ M)	24	13	4
9a	NPY ($1e^{-8}$ M) + CGP ($3e^{-8}$ M)	45	25	6	11f-g	Control	26	13	10
11a	Control	28	17	4	11f-g	AIP ($4e^{-8}$ M)	21	10	4
11a	CsA ($2e^{-9}$ M)	35	16	4	11f-g	AIP ($4e^{-8}$ M) + CRF ($3e^{-8}$ M)	21	11	4
11a	CsA ($2e^{-9}$ M) + NPY ($1e^{-8}$ M)	31	18	4					
11a	OA ($1e^{-8}$ M)	39	15	4					
11a	OA ($1e^{-8}$ M) + cPP ($1e^{-7}$ M)	38	15	4					
11e	Control	28	15	11					
11e	AIP ($4e^{-8}$ M)	27	13	4					
11e	AIP ($4e^{-8}$ M) + CRF ($3e^{-8}$ M)	29	14	4					

779 **Table 2. Numbers of neurons, OTCs and animals used for capacitance and morphological**
780 **analysis, indexed by Figure.**

781

782 **References**
783
784 Adamec, R., Hebert, M., Blundell, J. and Mervis, R.F. (2012). Dendritic morphology of amygdala
785 and hippocampal neurons in more and less predator stress responsive rats and more and less
786 spontaneously anxious handled controls. Behav. Brain Res. 226, 133-146. doi:
787 10.1016/j.bbr.2011.09.009
788
789 Avossa, D., Rosato-Siri, M.D., Mazzarol, F. and Ballerini, L. (2003). Spinal circuits formation: a
790 study of developmentally regulated markers in organotypic cultures of embryonic mouse spinal
791 cord. Neuroscience 122, 391-405.

792 Beck-Sickinger AG, Grouzmann E, Hoffmann E, Gaida W, van Meir EG, Waeber B, Jung G.
793 (1992). A novel cyclic analog of neuropeptide Y specific for the Y2 receptor. Eur. J. Biochem.
794 206:957-964.

795 Berglund, M.M., Schober, D.A., Statnick, M.A., McDonald, P.H. and Gehlert, D.R. (2003). The
796 use of bioluminescence resonance energy transfer 2 to study neuropeptide Y receptor agonist-
797 induced beta-arrestin 2 interaction. J. Pharmacol. Exp. Ther. 306, 147-156.
798
799 Böhme I, Stichel J, Walther C, Mörl K, Beck-Sickinger AG.(2008). Agonist induced receptor
800 internalization of neuropeptide Y receptor subtypes depends on third intracellular loop and C-
801 terminus. Cell Signal. 20:1740-1749 doi: 10.1016/j.cellsig.2008.05.017.
802
803 Cabrele, C. and Beck-Sickinger, A.G. (2000). Molecular characterization of the ligand-receptor
804 interaction of the neuropeptide Y family. J Pept Sci 6, 97-122.
805
806 Cabrele, C., Wieland, H.A., Langer, M., Stidsen, C.E. and Beck-Sickinger, A.G. (2001). Y-
807 receptor affinity modulation by the design of pancreatic polypeptide/neuropeptide Y chimera led
808 to Y(5)-receptor ligands with picomolar affinity. Peptides 22, 365-378.
809
810 Campeau, J.L., Wu, G., Bell, J.R., Rasmussen, J. and Sim, V.L.(2013). Early increase and late
811 decrease of purkinje cell dendritic spine density in prion-infected organotypic mouse cerebellar
812 cultures. PLoS One 8, e81776. doi: 10.1371/journal.pone.0081776.
813
814 Chee, M.J., Myers, M.G., Jr., Price, C.J. and Colmers, W.F. (2010). Neuropeptide Y suppresses
815 anorexigenic output from the ventromedial nucleus of the hypothalamus. J. Neurosci. 30, 3380-
816 3390. doi: 10.1523/JNEUROSCI.4031-09.2010.
817
818 Cohen P., Holmes, C.F., Tsukitani, Y. (1990) Okadaic acid: a new probe for the study of cellular
819 regulation. Trends Biochem Sci. 15:98-102.
820
821 De Simoni, A., Griesinger, C.B. and Edwards, F.A. (2003) Development of rat CA1 neurones in
822 acute versus organotypic slices: role of experience in synaptic morphology and activity. J.
823 Physiol. 550, 135-147.
824

825 Debanne, D., Gahwiler, B.H. and Thompson, S.M. (1999). Heterogeneity of synaptic plasticity at
826 unitary CA3-CA1 and CA3-CA3 connections in rat hippocampal slice cultures. J. Neurosci. 19,
827 10664-10671.
828
829 Ehrlich, D.E., Ryan, S.J. and Rainnie, D.G. (2012). Postnatal development of electrophysiological
830 properties of principal neurons in the rat basolateral amygdala. J. Physiol. 590, 4819-4838. oi:
831 10.1113/jphysiol.2012.237453
832
833 Ehrlich, D.E., Ryan, S.J., Hazra, R., Guo, J.D. and Rainnie, D.G. (2013). Postnatal maturation of
834 GABAergic transmission in the rat basolateral amygdala. J. Neurophysiol. 110, 926-941. doi:
835 10.1152/jn.01105.2012
836
837 File S.E. and Seth, P. (2003). A review of 25 years of the social interaction test. Eur J Pharmacol.
838 463:35-536.
839
840 Gahwiler, B.H. (1981). Morphological differentiation of nerve cells in thin organotypic cultures
841 derived from rat hippocampus and cerebellum. Proc. R. Soc. Lond. B. Biol. Sci. 211, 287-290.
842
843 Giesbrecht, C.J., Mackay, J.P., Silveira, H.B., Urban, J.H. and Colmers, W.F. (2010)
844 Countervailing modulation of Ih by neuropeptide Y and corticotrophin-releasing factor in
845 basolateral amygdala as a possible mechanism for their effects on stress-related behaviors. J.
846 Neurosci. 30, 16970-16982. doi: 10.1523/JNEUROSCI.2306-10.2010
847
848 Gutman, A.R., Yang, Y., Ressler, K.J. and Davis, M. (2008). The role of neuropeptide Y in the
849 expression and extinction of fear-potentiated startle. J. Neurosci. 28, 12682-12690. doi:
850 10.1523/JNEUROSCI.2305-08.2008.
851
852 Heilig, M., Koob, G.F., Ekman, R. and Britton, K.T. (1994). Corticotropin-releasing factor and
853 neuropeptide Y: role in emotional integration. Trends Neurosci. 17, 80-85.
854
855 Hill, M.N., Hillard, C.J. and McEwen, B.S. (2011). Alterations in corticolimbic dendritic
856 morphology and emotional behavior in cannabinoid CB1 receptor-deficient mice parallel the
857 effects of chronic stress. Cereb. Cortex 21, 2056-2064. doi: 10.1093/cercor/bhq280
858
859 Holliday, N.D., Lam, C.W., Tough, I.R. and Cox, H.M. (2005). Role of the C terminus in
860 neuropeptide Y Y1 receptor desensitization and internalization. Mol. Pharmacol. 67, 655-664.
861
862 Humpel, C. (2015). Organotypic brain slice cultures: A review. Neuroscience 305, 86-98. doi:
863 10.1002/cpim.59
864
865 Ishida, A., Kameshita, I., Okuno, S., Kitani, T. and Fujisawa, H. (1995). A novel highly specific
866 and potent inhibitor of calmodulin-dependent protein kinase II. Biochem. Biophys. Res. Commun.
867 212, 806-812.
868

869 Kim, H., Kim, E., Park, M., Lee, E. and Namkoong, K. (2013) Organotypic hippocampal slice
870 culture from the adult mouse brain: a versatile tool for translational neuropsychopharmacology.
871 Prog. Neuropsychopharmacol. Biol. Psychiatry 41, 36-43. doi: 10.1016/j.pnpbp.2012.11.004
872
873 Lin, CH, Yeh SH, Leu TH, Chang WC, Wang ST and Gean PW. (2003). Identification of
874 calcineurin as a key signal in the extinction of fear memory. J. Neurosci. 23, 1574-1579.
875
876 Liu, J., Farmer JD Jr, Lane WS, Friedman J, Weissman I and Schreiber SL. (1991). Calcineurin is
877 a common target of cyclophilin-cyclosporin A and FKBP-FK506 complexes. Cell 66, 807-815.
878
879 Lu, V.B., Colmers, W.F. and Smith, P.A.(2009). Long-term effects of brain-derived neurotrophic
880 factor on the frequency of inhibitory synaptic events in the rat superficial dorsal horn.
881 Neuroscience 161, 1135-1143. doi: 10.1016/j.neuroscience.2009.04.030.
882
883 Lu, V.B., Moran TD, Balasubramanyan S, Alier KA, Dryden WF, Colmers WF and Smith PA.
884 (2006). Substantia Gelatinosa neurons in defined-medium organotypic slice culture are similar to
885 those in acute slices from young adult rats. Pain 121, 261-275.
886
887 Mackay, J.P., Bompolaki M, DeJoseph MR, Michaelson SD, Urban JH and Colmers WF. (2019).
888 NPY2 Receptors Reduce Tonic Action Potential-Independent GABAB Currents in the Basolateral
889 Amygdala. J. Neurosci. 2019; 10.1523/Jneurosci.2226-18.2019 .
890
891 Marley, A., Choy, R.W. and von Zastrow, M. (2013). GPR88 reveals a discrete function of
892 primary cilia as selective insulators of GPCR cross-talk. PLoS One 8, e70857. doi:
893 10.1371/journal.pone.0070857.
894
895 McDonald, A.J. (1985). Immunohistochemical identification of gamma-aminobutyric acid-
896 containing neurons in the rat basolateral amygdala. *Neurosci. Lett.* **53**, 203-207.
897
898 McDonald, A.J., Beitz AJ, Larson AA, Kuriyama R, Sellitto C and Madl JE. (1989). Co-
899 localization of glutamate and tubulin in putative excitatory neurons of the hippocampus and
900 amygdala: an immunohistochemical study using monoclonal antibodies. *Neuroscience* **30**, 405-
901 421.
902
903 McEwen, B.S. (2003). Mood disorders and allostatic load. *Biol. Psychiatry* **54**, 200-207.
904
905 Michel, M.C., Beck-Sickinger A, Cox H, Doods HN, Herzog H, Larhammar D, Quirion R,
906 Schwartz T and Westfall T. (1989). XVI. International Union of Pharmacology recommendations
907 for the nomenclature of neuropeptide Y, peptide YY, and pancreatic polypeptide receptors.
908 Pharmacol. Rev. 50, 143-150.
909
910 Mineur, Y.S., Taylor, S.R. and Picciotto, M.R. (2014). Calcineurin downregulation in the
911 amygdala is sufficient to induce anxiety-like and depression-like behaviors in C57BL/6J male
912 mice. Biol. Psychiatry 75, 991-998. doi: 10.1016/j.biopsych.2014.03.009.
913

914 Mitra, R., Jadhav, S., McEwen, B.S., Vyas, A. and Chattarji, S. (2005) Stress duration modulates
915 the spatiotemporal patterns of spine formation in the basolateral amygdala. *Proc. Natl. Acad. Sci.*
916 *U. S. A.* **102**, 9371-9376.
917
918 Molosh, A.I., Sajdyk TJ, Truitt WA, Zhu W, Oxford GS and Shekhar A. (2013). NPY Y1
919 receptors differentially modulate GABAA and NMDA receptors via divergent signal-transduction
920 pathways to reduce excitability of amygdala neurons. Neuropsychopharmacology 38, 1352-1364.
921 doi: 10.1038/npp.2013.33.
922
923 Padival, M.A., Blume, S.R. and Rosenkranz, J.A. (2013) Repeated restraint stress exerts different
924 impact on structure of neurons in the lateral and basal nuclei of the amygdala. Neuroscience 246,
925 230-242. doi: 10.1016/j.neuroscience.2013.04.061
926
927 Pape, H.C. and Pare, D. (2010). Plastic synaptic networks of the amygdala for the acquisition,
928 expression, and extinction of conditioned fear. Physiol. Rev. 90, 419-463. doi:
929 10.1152/physrev.00037.2009
930
931 Paxinos, G. and Watson, C. (1986). The rat brain in stereotaxic coordinates (Academic Press,
932 Sydney;
933
934 Phelps, E.A. and LeDoux, J.E. (2005). Contributions of the amygdala to emotion processing: from
935 animal models to human behavior. Neuron 48, 175-187.
936
937 Rainnie, D.G., Bergeron R., Sajdyk T., Patil M., Gehlert D. and Shekhar A. (2004).
938 Corticotrophin releasing factor-induced synaptic plasticity in the amygdala translates stress into
939 emotional disorders. J. Neurosci. 24, 3471-3479.
940
941 Roozendaal, B., McEwen, B.S. and Chattarji, S. (2009). Stress, memory and the amygdala. *Nat.*
942 *Rev. Neurosci.* **10**, 423-433. doi: 10.1038/nrn2651
943
944 Sajdyk, T.J., Johnson PL, Leitermann RJ, Fitz SD, Dietrich A, Morin M, Gehlert DR, Urban JH,
945 and Shekhar A. (2008). Neuropeptide Y in the amygdala induces long-term resilience to stress-
946 induced reductions in social responses but not hypothalamic-adrenal-pituitary axis activity or
947 hyperthermia. J. Neurosci. 28, 893-903 (2008). doi: 10.1523/JNEUROSCI.0659-07.2008.
948
949 Sajdyk, T.J., Fitz, S.D. and Shekhar, A. (2006). The role of neuropeptide Y in the amygdala on
950 corticotropin-releasing factor receptor-mediated behavioral stress responses in the rat. Stress 9,
951 21-28.
952
953 Sajdyk, T.J., Schober, D.A. and Gehlert, D.R. (2002a). Neuropeptide Y receptor subtypes in the
954 basolateral nucleus of the amygdala modulate anxiogenic responses in rats. Neuropharmacology
955 43, 1165-1172.
956
957 Sajdyk, T.J., Schober, D.A., Smiley, D.L. and Gehlert, D.R. (2002b). Neuropeptide Y-Y2
958 receptors mediate anxiety in the amygdala. Pharmacol. Biochem. Behav. 71, 419-423.
959

960 Sajdyk, T.J., Shekhar, A. and Gehlert, D.R. (2004). Interactions between NPY and CRF in the
961 amygdala to regulate emotionality. Neuropeptides 38, 225-234.
962
963 Schmeltzer SN, Herman JP, **Sah R**. (2016) Neuropeptide Y (NPY) and posttraumatic stress
964 disorder (PTSD): A translational update. Exp Neurol. 284:196-210. Doi:
965 10.1016/j.expneurol.2016.06.020
966
967 Selcher, J.C., Xu, W., Hanson, J.E., Malenka, R.C. and Madison, D.V. (2012). Glutamate receptor
968 subunit GluA1 is necessary for long-term potentiation and synapse unsilencing, but not long-term
969 depression in mouse hippocampus. Brain Res. 1435, 8-14. doi: 10.1016/j.brainres.2011.11.029.
970
971 Sholl, D.A. (1953). Dendritic organization in the neurons of the visual and motor cortices of the
972 cat. J. Anat. 87, 387-406.
973
974 Silveira Villarroel, H., Bompolaki M, Mackay JP, Miranda Tapia AP, Michaelson SD,
975 Leitermann RJ, Marr RA, Urban JH and Colmers WF. (2018). NPY Induces Stress Resilience via
976 Downregulation of Ih in Principal Neurons of Rat Basolateral Amygdala. J. Neurosci. 38, 4505-
977 4520. doi: 10.1523/JNEUROSCI.3528-17.2018
978
979 Soll, R.M., Dinger, M.C., Lundell, I., Larhammer, D. and Beck-Sickinger, A.G. (2001). Novel
980 analogues of neuropeptide Y with a preference for the Y1-receptor. Eur. J. Biochem. 268, 2828-
981 2837.

982 Stanić D, Mulder J, Watanabe M, Hökfelt T. (2011). Characterization of NPY Y2 receptor protein
983 expression in the mouse brain. II. Coexistence with NPY, the Y1 receptor, and other
984 neurotransmitter-related molecules. J Comp Neurol. 519:1219-1257. doi: 10.1002/cne.22608.

985 Stoppini, L., Buchs, P.A. and Muller, D. (1991). A simple method for organotypic cultures of
986 nervous tissue. J. Neurosci. Methods 37, 173-182.
987
988 Taylor, A.L. (2012). What we talk about when we talk about capacitance measured with the
989 voltage-clamp step method. J. Comput. Neurosci. 32, 167-175 (2012). doi: 10.1007/s10827-011-
990 0346-8.
991
992 Vyas, A., Jadhav, S. and Chattarji, S. (2006). Prolonged behavioral stress enhances synaptic
993 connectivity in the basolateral amygdala. Neuroscience 143, 387-393.
994
995 Vyas, A., Mitra, R., Shankaranarayana Rao, B.S. and Chattarji, S. (2002). Chronic stress induces
996 contrasting patterns of dendritic remodeling in hippocampal and amygdaloid neurons. J. Neurosci.
997 22, 6810-6818.
998
999 Vyas, A., Pillai, A.G. and Chattarji, S. (2004). Recovery after chronic stress fails to reverse
1000 amygdaloid neuronal hypertrophy and enhanced anxiety-like behavior. Neuroscience 128, 667-
1001 673.
1002

1003 Wahlestedt C, Yanaihara N and Håkanson R. (1986). Evidence for different pre-and post-
1004 junctional receptors for neuropeptide Y and related peptides. Regul Pept. 13:307-318.
1005
1006 Yehuda R, Brand S, Yang RK. (2006). Plasma neuropeptide Y concentrations in combat exposed
1007 veterans: relationship to trauma exposure, recovery from PTSD, and coping. Biol Psychiatry.
1008 59:660-663.
1009
1010 Zhou Z, Zhu G, Hariri AR, Enoch MA, Scott D, Sinha R, Virkkunen M, Mash DC, Lipsky RH,
1011 Hu XZ, Hodgkinson CA, Xu K, Buzas B, Yuan Q, Shen PH, Ferrell RE, Manuck SB, Brown SM,
1012 Hauger RL, Stohler CS, Zubieta JK, Goldman D. (2008) Genetic variation in human NPY
1013 expression affects stress response and emotion. Nature 452:997-1001